iScience

CellPress
OPEN ACCESS

Article

STING Mediates Lupus via the Activation of Conventional Dendritic Cell Maturation and Plasmacytoid Dendritic Cell Differentiation

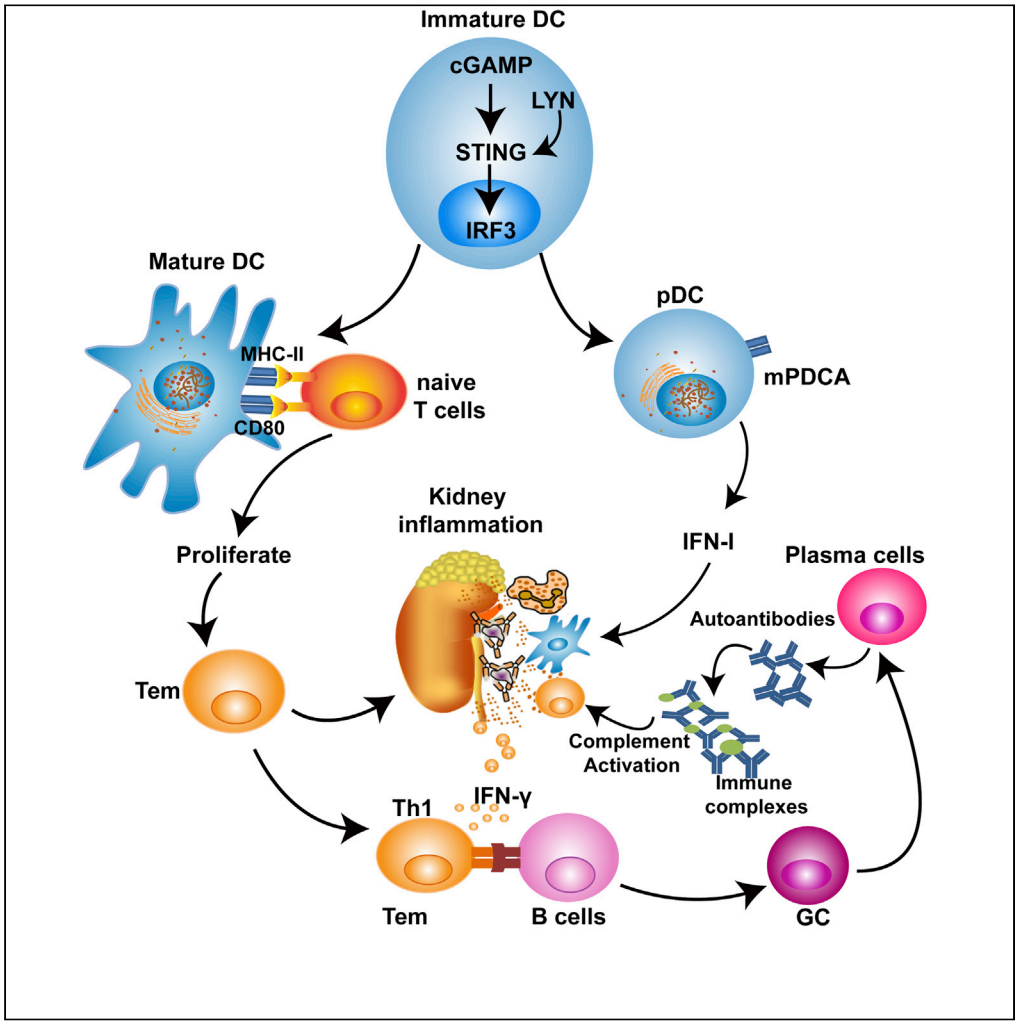

Arthid Thim-uam, Thaneas Prabakaran, Mookmanee Tansakul, ..., Søren Paludan, Trairak Pisitkun, Prapaporn Pisitkun

pisitkut@nhlbi.nih.gov (T.P.)
prapaporn.pis@mahidol.ac.th (P.P.)

HIGHLIGHTS

STING constitutively activates in the Fcgr2b-deficient lupus mice

Signaling through STING-LYN interaction promotes DC differentiation

Inhibition of STING pathway disrupts the lupus phenotypes

STING mediates lupus disease via the activation of dendritic cells

Thim-uam et al., iScience *23*, 101530
September 25, 2020
https://doi.org/10.1016/j.isci.2020.101530

iScience

CellPress
OPEN ACCESS

Article

STING Mediates Lupus via the Activation of Conventional Dendritic Cell Maturation and Plasmacytoid Dendritic Cell Differentiation

Arthid Thim-uam,[1,2] Thaneas Prabakaran,[3] Mookmanee Tansakul,[4] Jiradej Makjaroen,[2] Piriya Wongkongkathep,[2] Naphat Chantaravisoot,[2,5] Thammakorn Saethang,[2] Asada Leelahavanichkul,[6] Thitima Benjachat,[6] Søren Paludan,[3] Trairak Pisitkun,[2,7,*] and Prapaporn Pisitkun[4,8,9,*]

SUMMARY

Signaling through stimulator of interferon genes (STING) leads to the production of type I interferons (IFN-Is) and inflammatory cytokines. A gain-of-function mutation in STING was identified in an autoinflammatory disease (STING-associated vasculopathy with onset in infancy; SAVI). The expression of cyclic GMP-AMP, DNA-activated cGAS-STING pathway, increased in a proportion of patients with SLE. The STING signaling pathway may be a candidate for targeted therapy in SLE. Here, we demonstrated that disruption of STING signaling ameliorated lupus development in *Fcgr2b*-deficient mice. Activation of STING promoted maturation of conventional dendritic cells and differentiation of plasmacytoid dendritic cells via LYN interaction and phosphorylation. The inhibition of LYN decreased the differentiation of STING-activated dendritic cells. Adoptive transfer of STING-activated bone marrow-derived dendritic cells into the FCGR2B and STING double-deficiency mice restored lupus phenotypes. These findings provide evidence that the inhibition of STING signaling may be a candidate targeted treatment for a subset of patients with SLE.

INTRODUCTION

Systemic lupus erythematosus (SLE) is an autoimmune disease with characteristics of autoantibody production and immune complex deposition that lead to severe inflammation and fatal glomerulonephritis. The heterogeneity of lupus disease has been shown through several mouse models of lupus disease, suggesting a variety of unique mechanisms participating in its pathogenesis. Type I interferon (IFN-I) is known to play significant roles in SLE pathogenesis (Muskardin and Niewold, 2018). In many patients with SLE, the expression of interferon-inducible genes is increased in their peripheral blood mononuclear cells (Baechler et al., 2003). Nucleic acid-sensing pathways are the main contributors of IFN-I production (Paludan, 2015). Several studies suggest that inappropriate recognition of self-nucleic acids can induce the production of IFN-I and promote SLE disease (Muskardin and Niewold, 2018).

Nucleic acids derived from extracellular sources are sensed via endosomal Toll-like-receptors (TLRs), whereas the recognition of cytosolic nucleic acids is independent of TLRs (Keating et al., 2011). The activation of TLRs, such as TLR7 and TLR9, by endosomal nucleic acids, leads to type I interferon production (Asselin-Paturel et al., 2005). Spontaneous duplication of *Tlr7* causes autoimmune lupus phenotypes in *Yaa*-carrying BXSB mice (Pisitkun et al., 2006). Overexpression of *Tlr7* promotes autoimmunity through dendritic cell proliferation, whereas the deletion of *Tlr7* in lupus-prone MRL/*lpr* mice diminishes autoantibody and immune activation (Christensen et al., 2006; Deane et al., 2007). However, blocking TLR-mediated signaling by anti-malarial drugs can only treat SLE with mild disease activity (Sacre et al., 2012; Zeidi et al., 2019). Thus, investigation of other nucleic acid sensor pathways involved in lupus development could offer a more significant therapeutic opportunity.

Several cytosolic DNA sensors can induce IFN-I production, with cyclic GMP-AMP synthase (cGAS) being the major one (Sun et al., 2013). Cytosolic DNA sensing is also essential for innate immune signaling, and dysregulation of this process can cause autoimmune and inflammatory diseases (Yan, 2017). Stimulator of

[1]Interdisciplinary Program of Biomedical Sciences, Graduate School, Chulalongkorn University, 1873 Rama 4 Road, Pathumwan, Bangkok 10330, Thailand

[2]Center of Excellence in Systems Biology, Faculty of Medicine, Chulalongkorn University, 1873 Rama 4 Road, Pathumwan, Bangkok 10330, Thailand

[3]Department of Biomedicine, Aarhus University, Aarhus 8000, Denmark

[4]Section for Translational Medicine Program, Faculty of Medicine Ramathibodi Hospital, Mahidol University, 270 Rama 6 Road, Ratchathewi, Bangkok 10400, Thailand

[5]Department of Biochemistry, Faculty of Medicine, Chulalongkorn University, 1873 Rama 4 Road, Pathumwan, Bangkok 10330, Thailand

[6]Center of Excellence in Immunology and Immune-mediated Diseases, Faculty of Medicine, Chulalongkorn University, 1873 Rama 4 Road, Pathumwan, Bangkok 10330, Thailand

[7]Epithelial Systems Biology Laboratory, National Heart, Lung and Blood Institute, National Institutes of Health, Bethesda, MD, USA

[8]Division of Allergy, Immunology, and Rheumatology, Department of Medicine, Faculty of Medicine Ramathibodi Hospital, Mahidol University, 270 Rama 6 Road, Ratchathewi, Bangkok 10400, Thailand

[9]Lead Contact

*Correspondence: pisitkut@nhlbi.nih.gov (T.P.), prapaporn.pis@mahidol.ac.th (P.P.)

https://doi.org/10.1016/j.isci.2020.101530

interferon genes (STING), also known as transmembrane protein 173 (TMEM173), is a cytoplasmic adaptor protein that acts downstream of cGAS to enhance IFN-I production (Ishikawa et al., 2009). The loss-of-function mutations in a DNA-specific exonuclease gene *TREX1*, resulting in increased cytosolic DNA levels, are observed in the type I interferonopathies Aicardi-Goutieres syndrome (AGS) and chilblain lupus (Crow et al., 2006; Günther et al., 2013). Consistent with these scenarios in human, *Trex1*-deficient mice exhibit fatal inflammation and autoimmunity (Morita et al., 2004; Stetson et al., 2008). Inhibition of the STING pathway in these mice improves their inflammatory condition and survival (Ahn et al., 2014). Moreover, the absence of STING rescues embryonic lethality and arthritis development in another nuclease knockout model, i.e., *DNase II*-deficient mice (Ahn et al., 2012).

The spontaneous lupus mouse models commonly used to study SLE pathogenesis are MRL/*lpr*, NZBxNZW.F1, and BxSB (Theofilopoulos and Dixon, 1985). Since these models possess different genetic backgrounds, each model could develop lupus with unique pathogenesis (Murphy and Roths, 1979; Pisitkun et al., 2006; Theofilopoulos and Dixon, 1985). Surprisingly, the absence of STING in MRL/*lpr* mice does not improve lupus phenotypes but instead promotes more inflammation (Sharma et al., 2015). Furthermore, knocking down the IFN receptor gene *Ifnar1* in MRL/*lpr* mice aggravates lymphoproliferation, autoantibody production, and end-organ damage (Hron and Peng, 2004; Nickerson et al., 2010). Although the expression of cyclic GMP-AMP, DNA-activated cGAS-STING pathway, activated IFN-I, and increased in a proportion of patients with SLE (An et al., 2017), the data from lupus mouse models reveal the differential roles of STING in lupus pathogenesis depending on the models. Therefore, further studies in a relevant animal model that reflects human lupus are required to circumvent these conflicting data.

A comprehensive genetic analysis has identified *FCGR2B* as a susceptibility gene in patients with SLE (Zhu et al., 2016). The deletion of the *Fcgr2b* gene causes a lupus-like disease in genetic susceptibility to autoimmune development. The *Fcgr2b*$^{-/-}$ mice created in 129 strain with subsequently backcrossed into C57BL/6 develop overt autoreactivity and fatal lupus disease while the deletion of *Fcgr2b* in C57BL/6 mice showed only autoantibody production (Bolland and Ravetch, 2000; Boross et al., 2011). The 129-derived Sle16 covering the Nba2 interval region is an autoimmune susceptibility locus, which contains the *Fcgr2b*, Slam family, interferon-inducible Ifi200 family genes (Boross et al., 2011; Choubey, 2012; Sato-Hayashizaki et al., 2011). Among the Ifi200 family, the *Ifi202* shows the highest expression in the splenocytes from Nba2 carrying mice (Rozzo et al., 2001). The *Ifi202* is a candidate lupus susceptibility gene, and its human homolog *IFI16* shows the association with SLE (Kimkong et al., 2010). Also, IFI16 signals through STING to initiate IFN-I production (Choubey and Panchanathan, 2008; Unterholzner et al., 2010). Based on the genetic background of the 129-derived locus, STING may play a significant role in the pathogenesis of the 129/B6.*Fcgr2b*$^{-/-}$ lupus mice.

In this work, we showed an increase in *Sting* expression of the 129/B6.*Fcgr2b*$^{-/-}$ mice. Disruption of STING signaling rescued lupus phenotypes of the 129/B6.*Fcgr2b*$^{-/-}$ mice. Stimulation of STING promoted dendritic cell maturation and plasmacytoid dendritic cell differentiation. After STING activation, LYN was phosphorylated and recruited to interact with STING. Inhibition of LYN diminished STING-driven differentiation of dendritic cells. The adoptive transfer of STING-activated bone marrow-derived dendritic cells (BMDCs) into the double-deficiency (*Fcgr2b*$^{-/-}$.*Sting*$^{gt/gt}$) mice restored the lupus phenotypes. The data suggested that STING signaling in the dendritic cells initiated the autoimmune development in the 129/B6.*Fcgr2b*$^{-/-}$ mice. STING is a promising therapeutic target for lupus disease.

RESULTS

Loss of the Stimulator of Type I Interferon Genes (STING) Increases Survival of *Fcgr2b*$^{-/-}$ Lupus Mice

First, we confirmed that 129/B6.*Fcgr2b*$^{-/-}$ mice (or *Fcgr2b*$^{-/-}$ in short) showed the increase of *Sting mRNA expression and protein expression in the spleen* (Figures 1A and 1B). We further observed the significant rise of mRNA expression of interferon-inducible genes (*Irf3, Irf7, Mx1*) (*Ifn-γ, Ifn-β,* and *Cxcl10*) and in the spleen of the *Fcgr2b*$^{-/-}$ mice (Figures 1C–1H). To determine whether the Sting signaling is required for lupus development in the *Fcgr2b*$^{-/-}$ mice, we generated the double deficiency of *Fcgr2b* and *Sting* together with control littermates. The *Fcgr2b*$^{-/-}$ mice were crossed with the C57BL/6.*Sting* deficiency or Goldenticket mice (*Sting*^{gt}), which behave as a functional knockout of STING (Sauer et al., 2011). Furthermore, we detected the increase of cGAMP in the splenocytes of the *Fcgr2b*$^{-/-}$.*Sting*$^{wt/gt}$ mice but not in the double-deficient mice (Figure 1I). The double-deficient mice (*Fcgr2b*$^{-/-}$.*Sting*$^{gt/gt}$) showed a higher

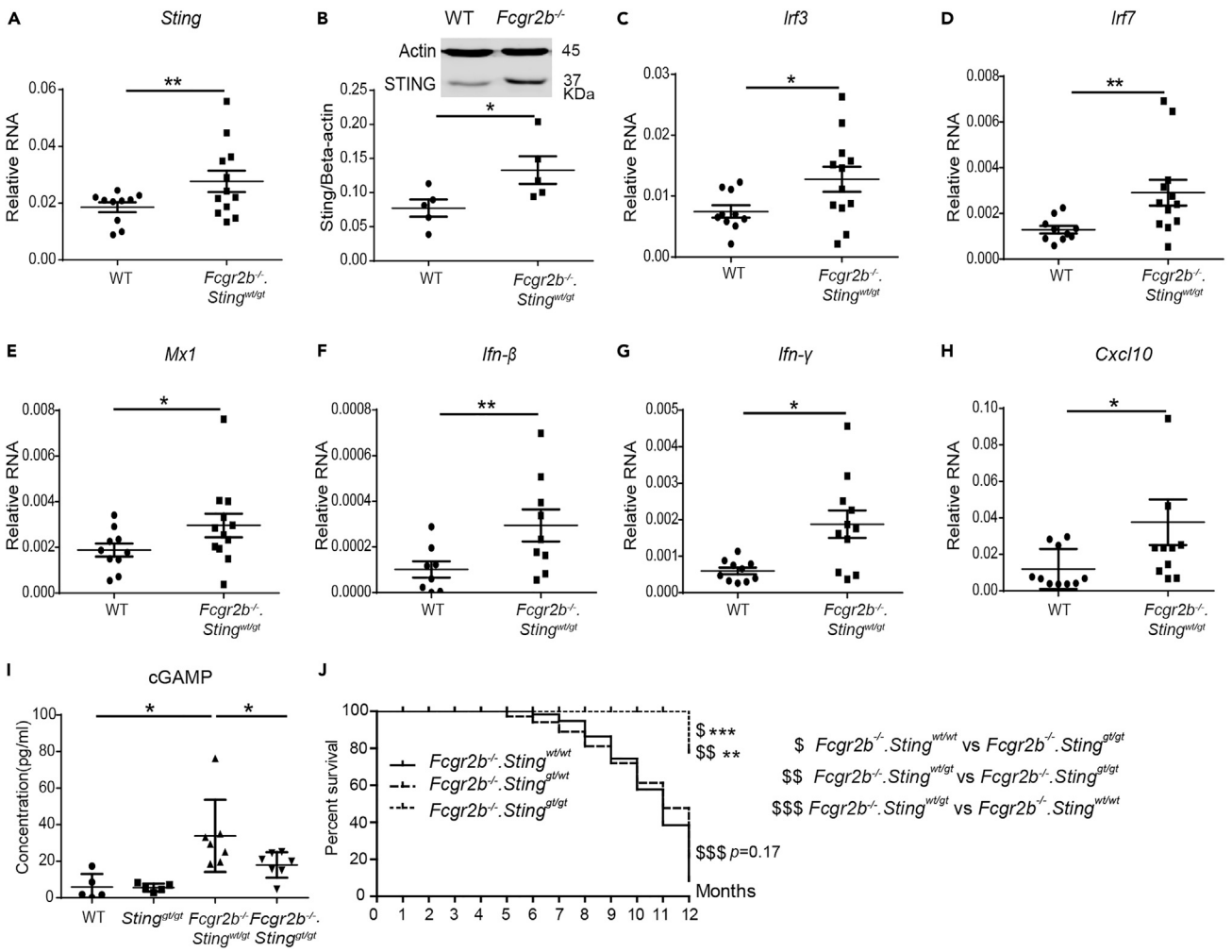

Figure 1. Loss of the Stimulator of Type I Interferon Genes (STING) Increases Survival of *Fcgr2b*$^{-/-}$ Lupus Mice

(A and C–H) Gene expression profiles from spleens of wild-type and *Fcgr2b*$^{-/-}$ mice at the age of 6 months were tested by real-time PCR (N = 10–12 per group). The relative RNA expressions (normalized by actin) of (A) *Sting*, (C) *Irf3*, (D) *Irf7*, (E) *Mx1*, (F) *Ifn-β*, (G) *Ifn-γ*, and (H) *Cxcl10* are shown.

(B) Isolated splenocytes were analyzed for STING protein expression by western blot. Data are representative of three mice per group. Quantification of the intensity was normalized by actin (N = 3 per group).

(I) The concentration of cGAMP from isolated splenocytes (N = 5–7).

(J) The *Fcgr2b*-deficient mice were crossed with *Sting*-deficient mice (*Sting*$^{gt/gt}$) to generate the double-deficient mice (*Fcgr2b*$^{-/-}$. *Sting*$^{gt/gt}$) and littermate controls. The survival curve of the mice was observed for up to 12 months (N = 14 per group).

Error bars indicate SEM; *p < 0.05, **p < 0.01, and ***p < 0.001. The dollar sign ($) shown the comparison between the group.

survival rate compared with the *Fcgr2b*$^{-/-}$ with homozygote *Sting* WT mice (Figure 1J). Also, the *Fcgr2b*$^{-/-}$ with heterozygote of Sting (*Sting*$^{wt/gt}$) showed similarity in phenotypes and survival with *Fcgr2b*$^{-/-}$ with wild-type Sting (*Sting*$^{wt/wt}$).

STING Signaling Pathway Promotes Autoantibody Production and Glomerulonephritis in the *Fcgr2b*$^{-/-}$ Lupus Mice

The lupus phenotypes of the double-deficient mice were examined and compared with littermate controls. The levels of the anti-nuclear antibody (ANA) and anti-dsDNA antibody from the sera of the double-deficient mice (*Fcgr2b*$^{-/-}$.*Sting*$^{gt/gt}$) were significantly lower than in the *Fcgr2b*$^{-/-}$ mice (Figures 2A–2C). The kidneys of *Fcgr2b*$^{-/-}$ mice showed pathology of diffuse proliferative glomerulonephritis, which did not present in the *Fcgr2b*$^{-/-}$.*Sting*$^{gt/gt}$ mice (Figure 2D). The glomerular and interstitial scores in the kidneys of *Fcgr2b*$^{-/-}$ mice were significantly higher than in the double-deficient mice (Figures 2E and 2F).

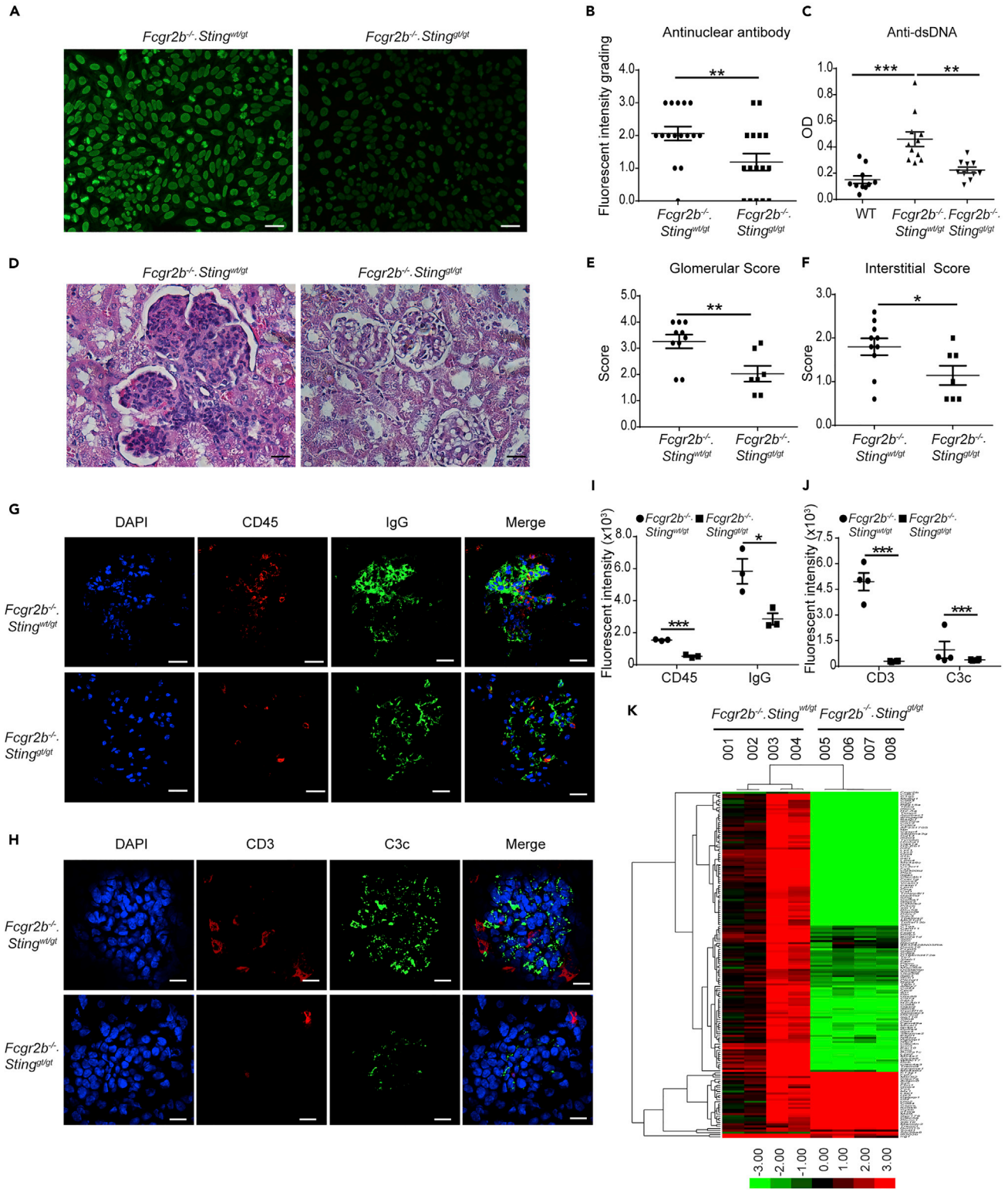

Figure 2. STING Signaling Pathway Promotes Autoantibody Production and Glomerulonephritis in the *Fcgr2b*$^{-/-}$ Lupus Mice

(A)The anti-nuclear antibodies (ANA) were detected in the serum (dilution 1:800) using the immunofluorescence staining on Hep-2 cells (A). Data are representative of eight mice per group (scale bar, 20 μm).

(B) Semi-quantification of ANA was graded by fluorescence intensity (N = 8 mice per group).

Figure 2. *Continued*

(C) Anti-dsDNA from sera (dilution 1:100) of *Fcgr2b*$^{-/-}$ and *Fcgr2b*$^{-/-}$. *Sting*$^{gt/gt}$ was detected by ELISA (N = 10–11 per group).

(D) Kidney sections of *Fcgr2b*$^{-/-}$ and *Fcgr2b*$^{-/-}$. *Sting*$^{gt/gt}$ mice (6–8 months old) were stained with H&E. Data are representative of 7–10 mice per group (scale bar, 25 μm).

(E–H) (E and F) Glomerular scores and interstitial scores of kidney sections were blindly graded (N = 7–10 per group). Immunofluorescence staining of the kidneys from *Fcgr2b*$^{-/-}$ and *Fcgr2b*$^{-/-}$. *Sting*$^{gt/gt}$ mice show in (G) IgG (green), CD45 (red), and DAPI (blue) and (H) C3c (green), CD3 (red), and DAPI (blue). Data are representative of 3–4 mice per group (scale bar, 10 μm).

(I and J) The quantitative immunofluorescence signal (I) CD45, and IgG, (J) CD3 and C3c (N = 3–4 mice per group). Data are shown as mean ± SEM; *p < 0.05, **p < 0.01 and ***p < 0.001.

(K) A heatmap of microarray data from the kidneys of *Fcgr2b*$^{-/-}$ and *Fcgr2b*$^{-/-}$. *Sting*$^{gt/gt}$ mice show that the interferon signature genes significantly changed in the *Fcgr2b*$^{-/-}$mice (N = 4 mice per group). Data shown in $\log_2$ (sample/wild-type).

Consistent with the pathology, the immunofluorescence staining showed fewer CD45$^+$ cells and IgG deposition in the kidneys of *Fcgr2b*$^{-/-}$.*Sting*$^{gt/gt}$ mice (Figures 2G and 2I). The cell types infiltrated in the kidneys of the *Fcgr2b*$^{-/-}$ mice were CD3$^+$ and CD11c$^+$ cells, which significantly reduced in the double-deficient mice (Figures 2H, 2J, S1B, and S1C. Related to Figure 2).

We further looked at the gene expression profiles in the kidney of these mice and found a significantly different expression (Figure S1A. Related to Figure 2). The expression of interferon-inducible genes in the kidney of these mice was higher in the *Fcgr2b*$^{-/-}$ mice, especially in the ones with greater severity (#003, 004), and there was a significant reduction of interferon-inducible genes in the kidneys of *Fcgr2b*$^{-/-}$.*Sting*$^{gt/gt}$ mice (Figure 2K). However, not all of these interferon-inducible genes decreased in the *Fcgr2b*$^{-/-}$.*Sting*$^{gt/gt}$ mice (Figure 2K). These data suggested that STING-dependent pathology mediated by both interferon and non-interferon signaling and not all of the interferon signaling in the *Fcgr2b*$^{-/-}$ mice contributed by the STING pathway.

STING Is Essential for Inflammatory Phenotypes of the *Fcgr2b*$^{-/-}$ Lupus Mice

The expression of interferon-inducible genes and interferon regulatory factors in the kidneys was confirmed by real-time PCR. The expressions of *Isg15*, *Mx1*, *Irf7*, and *Irf3* were upregulated in the *Fcgr2b*$^{-/-}$ mice and downregulated in the absence of STING (Figures 3A–3D). Also, the expression of *Irf5*, the lupus susceptibility gene, which upregulated in the kidneys of the *Fcgr2b*$^{-/-}$ mice, was Sting dependent (Figure S2A. Related to Figure 3). The splenocytes were analyzed from the mice at the age of 6–7 months to characterize the immunophenotypes. The expansion of dendritic cells (CD11c$^+$) and plasmacytoid dendritic cells (CD11c$^+$PDCA$^+$) in the *Fcgr2b*$^{-/-}$ mice diminished in the absence of Sting (Figures 3E and 3F). The reduction of T effector memory cells (CD3$^+$CD4$^+$CD62L^{lo}CD44^{hi}), germinal center B cells (B220$^+$GL7$^+$), and CD4$^+$ICOS$^+$ cells in the double-deficient mice were detected (Figures 3G, 3H, and S2B. Related to Figure 3). The percentage of IAb$^+$ B cells significantly reduced in the double-deficient mice (Figure S2C. Related to Figure 3). However, the expansion of plasma cells did not show the difference between single and double-deficient mice (Figure S2D. Related to Figure 3). Besides, the percentage of CD11b$^+$CD11c$^-$ and F480$^+$ cells did not increase in both *Fcgr2b*$^{-/-}$.*Sting*$^{wt/gt}$ mice and double-deficient mice (Figures S2E and S2F. Related to Figure 3). Furthermore, the sera levels of MCP-1 and TNF-α from the *Fcgr2b*$^{-/-}$.*Sting*$^{wt/gt}$ mice were significantly increased compared with WT mice (Figures 3I and 3J), whereas IL-1β and IL-23 did not show significant changes (Figures 3K and 3L). However, the levels of TNF-α, IL-1β, and IL-23 from the *Fcgr2b*$^{-/-}$ mice significantly decreased in the absence of STING (Figures 3J–3L). These data suggested that STING mediated the inflammatory process in the *Fcgr2b*-deficient lupus mice.

STING-Activated Dendritic Cells Induce the Proliferation of Naive CD4$^+$ T Cells

The splenocytes of Fcgr2b−/− mice showed an increase of effector memory T cells (Tem) and Ifng expression (Figures 3G and 1G). We hypothesized that the high proportion of Tem in the Fcgr2b−/− mice might contribute to the increase of Ifng expression. We performed the intercellular staining of IFN-γ to test this assumption. The IFN-γ$^+$CD4$^+$ T cells from the lymph nodes of Fcgr2b−/− mice were higher than wild-type and double-deficient mice (Figures 4A–4C). These IFN-γ$^+$CD4$^+$ T cells isolated from lymph nodes were primed *in vivo* by DCs. The reduction of IFN-γ$^+$CD4$^+$ T cells in the double-deficient mice could suggest that either STING in T cells or DCs could play a role in the *in vivo* Th1 skewing.

Sting deficiency reduced the DC expansion in the spleen of Fcgr2b−/− mice (Figure 3E). We hypothesized that DC of the Fcgr2b−/− mice might promote the expansion of Tem and IFN-γ$^+$ T cells. Thus, we

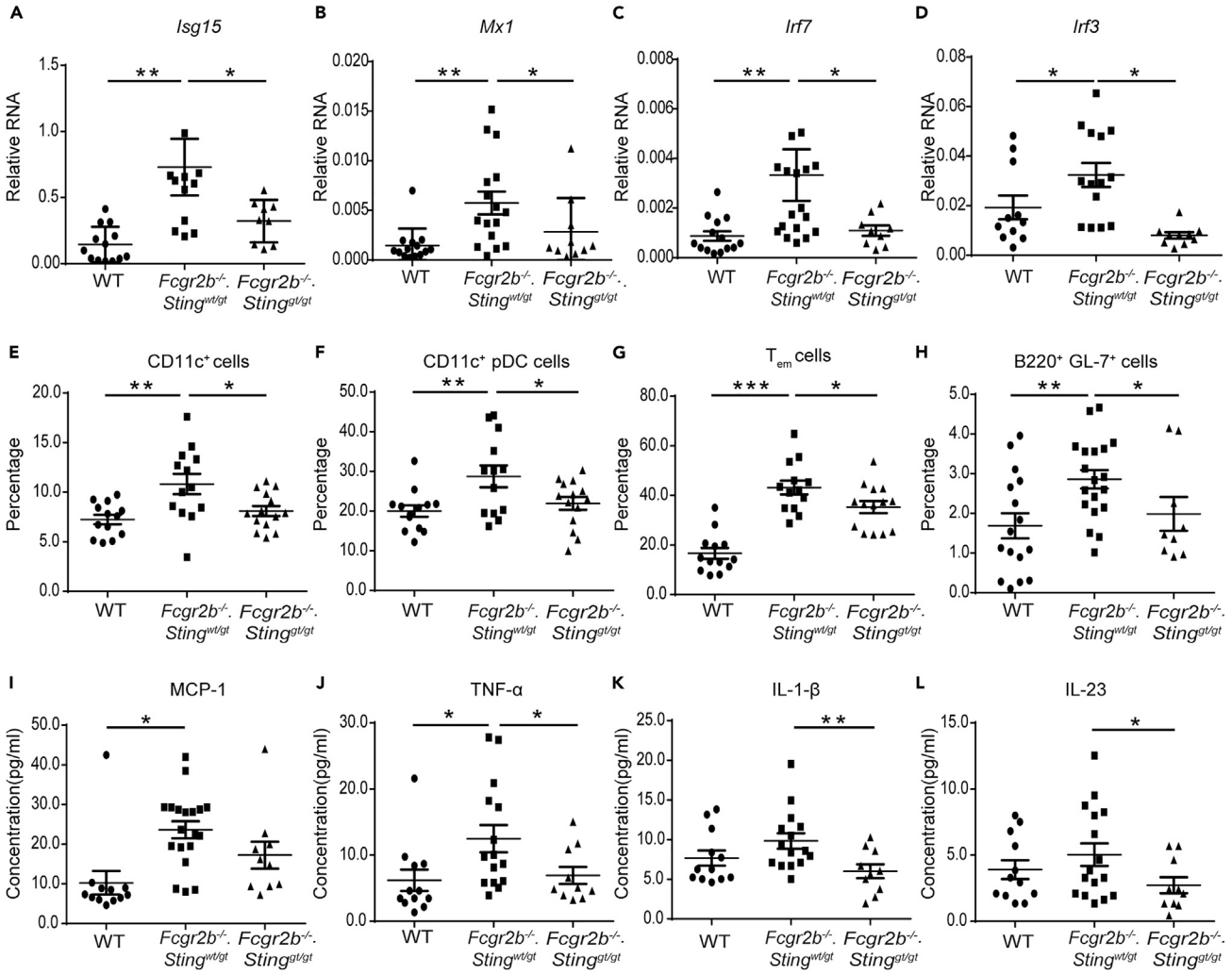

Figure 3. STING is Essential for Inflammatory Phenotypes of the *Fcgr2b*$^{-/-}$ Lupus Mice

(A–D) The relative RNA expression (normalized by actin) of (A) *Isg15*, (B) *Mx1*, (C) *Irf7*, and (D) *Irf3* from the kidneys of wild-type, *Fcgr2b*$^{-/-}$. *Sting*$^{wt/gt}$, and *Fcgr2b*$^{-/-}$. *Sting*$^{gt/gt}$ mice at the age of 6 months are shown (N = 10–17 per group).

(E–H) Flow cytometry analysis of splenocytes isolated from wild-type, *Fcgr2b*$^{-/-}$. *Sting*$^{wt/gt}$, and *Fcgr2b*$^{-/-}$. *Sting*$^{gt/gt}$ mice at the age of 6–7 months (N = 13–14 per group). Data are shown in the percentage of (E) CD11c^{+}, (F) plasmacytoid dendritic cells (pDC), (G) T_{em} ($CD3^{+}CD4^{+}CD44^{hi}CD62L^{lo}$), and (H) $B220^{+}GL7^{+}$ cells.

(I–L) The sera cytokines of wild-type, *Fcgr2b*$^{-/-}$. *Sting*$^{wt/gt}$, and *Fcgr2b*$^{-/-}$. *Sting*$^{gt/gt}$ mice at the age of 6 months were analyzed by cytometric bead array. Serum cytokines of (I) MCP-1, (J) TNF-α, (K) IL-1β, and (L) IL-23 (N = 10–15 per group).

Data are shown as mean ± SEM; *p < 0.05, **p < 0.01 and ***p < 0.001.

co-cultured T cells with BMDC to check if the STING-expressing DC could directly influence the IFN-γ production in T cells. The co-culture for 6 h between $CD4^{+}$ T cells (from every genotype) and STING-activated BMDC from either Fcgr2b−/− or double-deficient mice showed similar numbers of IFN-$\gamma^{+}CD4^{+}$ T cells (Figures 4D and 4E). However, the number of IFN-$\gamma^{+}CD4^{+}$ T cells isolated from Fcgr2b−/− mice in the co-culture with BMDC was higher than the isolated $CD4^{+}$ cells from double-knockout mice regardless of STING expression on BMDC (Figures 4D and 4E). These data suggested that T cell priming of whole $CD4^{+}$ T cells by DCs was not affected by the presence or absence of STING because Th1 cells in *Fcgr2b*$^{-/-}$ T cells were fully differentiated *in vivo*. This experiment suggested that STING-expressing DC could not promote the primed T cells *in vivo* to produce more IFN-γ.

Next, we tested if STING-expressing DC could prime naive T cells to proliferate and differentiate into IFN-γ-producing T cells. The purified naive T cells were labeled with CFSE and co-cultured with

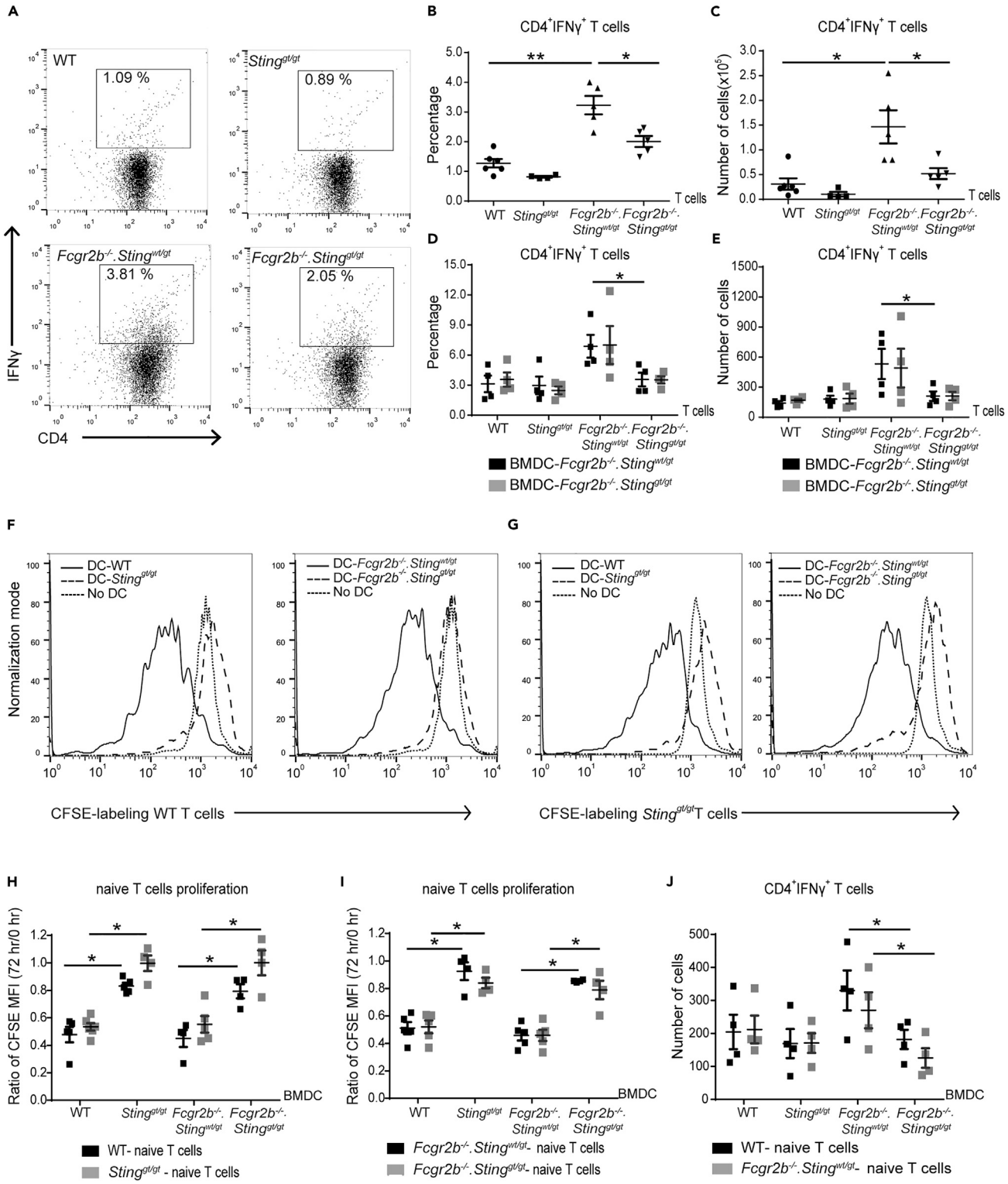

Figure 4. STING-Activated Dendritic Cells Induce the Proliferation of Naive CD4$^+$ T Cells

(A–C) Flow cytometry analysis of (A and B) intracellular staining of IFN-γ-producing CD4$^+$ T cells isolated from lymph nodes of wild-type, *Sting*$^{gt/gt}$, *Fcgr2b*$^{-/-}$.*Sting*$^{wt/gt}$, and *Fcgr2b*$^{-/-}$.*Sting*$^{gt/gt}$ mice at the age of 6–7 months. (A) Data are representative of 4–5 mice per group. (B) The percentage of IFN-γ$^+$CD4$^+$ T cells and (C) the number of IFN-γ$^+$CD4$^+$ T cells (N = 4–5 per group).

Figure 4. *Continued*

(D and E) The isolated CD4$^+$ T cells were co-cultured with stimulated BMDC for 6 h. The x axis shows the genotypes that CD4$^+$ T cells were isolated. (D) The percentage and (E) the number of intracellular IFN-γ-producing CD4$^+$ cells after co-culturing with DMXAA-activated BMDC from *Fcgr2b*$^{-/-}$.*Sting*$^{wt/gt}$ and *Fcgr2b*$^{-/-}$.*Sting*$^{gt/gt}$ (6–7 months old) for 6 h (N = 4–5).

(F–J) Co-culture of naive T cells with DMXAA-activated BMDC from wild-type, *Sting*$^{gt/gt}$, *Fcgr2b*$^{-/-}$.*Sting*$^{wt/gt}$, and *Fcgr2b*$^{-/-}$.*Sting*$^{gt/gt}$ mice for 72 h. The x axis shows the genotypes that BMDCs were isolated. (F and G) The histogram of CFSE labeling T cells in the co-culture with BMDCs. Data are representative of 4–5 mice per group. (H and I) CFSE dilution of isolated naive T cells showed in the ratio of mean fluorescence intensity (MFI) at 72 h/initial labeling (time 0), and (J) the total numbers of IFN-γ$^+$CD4$^+$ T cells (N = 4 per group).

Data are shown as mean ± SEM; *p < 0.05, and **p < 0.01.

STING-activated BMDC for 72 h. The CFSE dilution assay showed that STING-expressing DC induced the proliferation of naive T cells regardless of STING expression on T cells (Figures 4F–4I). Interestingly, only BMDC from the Fcgr2b−/− mice induced the differentiation of Th1 cells regardless of the STING expression on naive T cells (Figure 4J). These co-culture experiments indicated that intrinsic STING expression on DC, but not on T cells, promoted Th1 differentiation. The data suggested that STING activation promoted the maturation of DC in the Fcgr2b−/− mice, which subsequently primed the naive CD4$^+$ T cells to proliferate and become the IFN-γ-producing T cells.

STING Activation Promotes the Maturation of Dendritic Cells and the Differentiation of Plasmacytoid Dendritic Cells

The cGAS/STING pathway is essential for DC activation (Marinho et al., 2018). STING-activating DC can induce naive T cells to proliferate and produce IFN-γ (Figures 4H–4J), which suggested STING may enhance the maturation of DC to become professional antigen-presenting cells. We hypothesized that STING signaling could mediate the expansion of DC in the *Fcgr2b*$^{-/-}$ mice. The bone-marrow-derived dendritic cells (BMDCs) were differentiated into immature DCs and subsequently stimulated with STING ligands (DMXAA), DMSO, and LPS (as a control) to assess if STING played a role in DC maturation. The LPS control induced the immature DC to increase the expression of MHC-II (IA-b) and CD80, which suggested the phenotypes of mature DC, from both *Sting*-sufficient and *Sting*-deficient mice (Figures 5A and 5C). The immature DC from wild-type and *Fcgr2b*$^{-/-}$ mice also showed the increasing percentage of IA-b$^+$ and CD80$^+$ DC cells after DMXAA stimulation; the *Sting*-deficient mice did not develop these mature phenotypes (Figures 5B and 5D). The supernatant from BMDC culture with DMXAA stimulation showed an increase in the concentration of IL-1α, IL-6, TNF-α, and MCP-1 in the wild-type and *Fcgr2b*$^{-/-}$ mice but not in *Sting*-deficient mice and double-deficient mice (Figures 5E–5H).

To better understand the mechanisms of STING in DC differentiation, we performed the proteomic analysis of STING-activated BMDC in the *Fcgr2b*$^{-/-}$ mice compared with the double-deficient mice. The volcano plot showed the proteins that were highly expressed were interferon-regulated proteins (Figure 5I and Table S1. Lists of up and down of regulated proteins. Related to Figure 5). This finding may result from the increase of IFN-I production in the culture medium, which could upregulate the interferon-regulated proteins. We hypothesized that STING might promote the differentiation of pDC (a significant producer of IFN-I). The *in vitro* culture of BMDC with DMXAA and LPS (as a control) showed a significant increase in pDC and IFN-β with DMXAA but not with LPS stimulation (Figures 5K–5N). Also, we demonstrated the morphology of these cells by the imaging flow cytometry and found the pDCs expressed CD80 as well (Figure 5J). To confirm that activation of STING via another ligand results in DC differentiation, we stimulated the BMDC with cGAMP. The stimulation of STING with cGAMP increased the amount of CD11c$^+$IAb$^+$ (Figure S3A. Related to Figure 5), CD11c$^+$CD80$^+$ (Figure S2B. Related to Figure 5), and mPDCA$^+$ cells (Figure S3C. Related to Figure 5). These data suggested that the STING signaling pathway mediated DC maturation and pDC differentiation.

STING Activation Induced DC Maturation and Promoted the Interaction between LYN and STING in DC

STING-interacting proteins were identified by immunoprecipitation (IP) using the STING antibody that targets the N-terminal region of the protein. STING-activating BMDC with DMXAA for 3 h was immunoprecipitated and analyzed by mass spectrometry (Table S2. Lists of STING interacting proteins. Related to Figure 6). Among the proteins detected, LYN, a member of Src family kinases, has been shown to function in the maturation of DC and pDC response (Chu and Lowell, 2005; Dallari et al., 2017). Immunoprecipitation confirmed that LYN interacted with STING after DMXAA stimulation in WT BMDC, whereas LYN

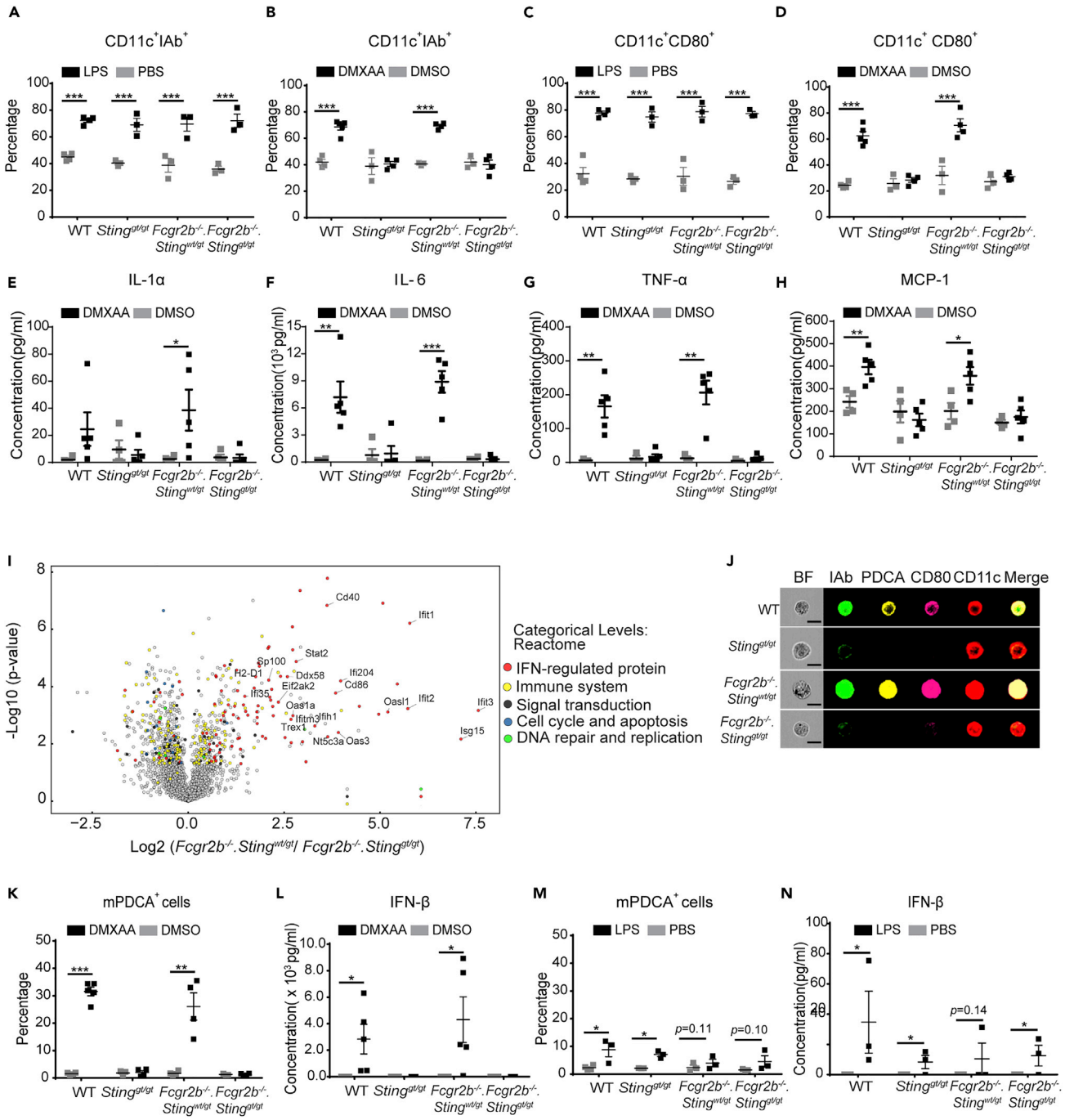

Figure 5. STING Activation Promotes the Maturation of Dendritic Cells and the Differentiation of Plasmacytoid Dendritic Cells

Bone marrows were isolated from wild-type, *Sting*$^{gt/gt}$, *Fcgr2b*$^{-/-}$. *Sting*$^{wt/gt}$, and *Fcgr2b*$^{-/-}$. *Sting*$^{gt/gt}$ mice at the age of 6 months.

(A–D) IL-4 and G-CSF differentiated bone marrow-derived dendritic cells (BMDC) for 5 days were stimulated with LPS or DMXAA for 24 h. Flow cytometry analysis shows the percentage of (A and B) CD11c^{+} IAb^{+} cells and (C and D) CD11c^{+}CD80^{+} cells.

(E–H) Supernatants were collected and analyzed after DMXAA stimulation for 24 h. Cytometric bead array shows the levels of (E) IL-1α, (F) IL-6, (G) TNF-α, and (H) MCP-1.

(I) Volcano plot of protein expressions from proteomic analysis of DMXAA-activated BMDC of *Fcgr2b*$^{-/-}$. *Sting*$^{wt/gt}$, and *Fcgr2b*$^{-/-}$.*Sting*$^{gt/gt}$ mice at the age of 6–7 months (N = 4 per group).

(J) Imaging flow cytometry of DMXAA-activated BMDC shows the representative staining of IAb (green), mPDCA (yellow), CD80 (pink), and CD11c (red) (N = 3 mice per group).

Figure 5. *Continued*
(K and M) The percentage of pDC (PDCA$^+$ cells) after (K) DMXAA activation and (M) LPS activation for 24 h (N = 3–4 per group).
(L and N) The level of IFN-β from the culture supernatant of activated BMDC with (L) DMXAA and (N) LPS (N = 5 per group).
Data are shown as mean ± SEM; *p < 0.05, **p < 0.01 and ***p < 0.001.

constitutively interacted with STING in the *Fcgr2b*-deficient BMDC (Figures 6A and 6C). This interaction could result from the intrinsic activation of STING in the *Fcgr2b*$^{-/-}$ mice. This activation did not change the protein abundance of LYN and STING in total cell lysate (Figures 6B and 6D). Also, the western blot from both IP and cell lysate showed another fainting band of STING after the activation; this protein was identified by mass spectrometry as the phosphorylation of STING (Ser357) (Figures S4A–S4B. Related to Figure 6). The activation of STING increased the phosphorylation of LYN (Tyr507) and AKT (Ser473), which were inhibited by PP2 (Figures 6E and S5D–S5E. Related to Figure 6).

Lyn kinase regulates DC maturation, and genetic deletion of *Lyn* ablates pDC (Chu and Lowell, 2005; Dallari et al., 2017). We hypothesized that STING promoted DC maturation and pDC differentiation through LYN signaling pathway, and the inhibition of LYN should affect the STING-induced BMDC differentiation. The *in vitro* data showed that pan SFK inhibitor PP2 decreased STING-mediated expression of IAb and CD80 on conventional DC (Figures 6F, 6G, and S4C. Related to Figure 6) and the differentiation of pDC (Figure 6H). Next, we tested whether PP2 inhibited STING-mediated signaling. The PP2 decreased the mRNA expression of *Irf3*, *Irf7*, *Isg15*, and *Cxcl10* in the STING-stimulated BMDC (Figures 6I–6L). These data suggested that PP2 treatment reduced the enhanced expression of ISG via STING activation.

To confirm the physical interaction between STING and LYN, we identified the colocalization of STING and LYN in the BMDC using two different clones of anti-STING and anti-LYN antibodies (Figures 6N and S5A. Related to Figure 6). The quantification of fluorescence signaling showed a significant increase in colocalization of STING and LYN upon STING stimulation (Figures 6M and S5C. Related to Figure 6). The *Fcgr2b*-deficient BMDC constitutively showed a certain degree of the colocalization between STING and LYN, whereas the activation of STING promoted more interaction (Figure 6N). Also, FYN, a member of the Src family kinases (SFKs), has been shown to have functional role in pDC maturation and PP2 inhibited both LYN and FYN signaling (Dallari et al., 2017). Therefore, we identified if FYN colocalized with STING and found that FYN did not colocalize with STING (Figure S5B. Related to Figure 6). These data suggested that activation of STING induced LYN interaction and mediated maturation and differentiation of conventional DCs and pDCs.

Adoptive Transfer of *Sting*-Expressing BMDC Induces Lupus Development in the *Fcgr2b*$^{-/-}$.*Sting*$^{gt/gt}$ Mice

The STING signaling pathway activated the immature BMDC to differentiate into the mature DC and pDC. The dendritic cells are significant producers of inflammatory cytokines and capable of promoting T cell proliferation and differentiation. We proposed that STING may induce the lupus disease by initially acting through the DC activation. We performed the adoptive transfer of the STING-activated BMDC derived from *Fcgr2b*$^{-/-}$ mice into WT recipient mice to test this hypothesis. The recipient WT mice developed the autoimmune phenotypes, including the production of anti-dsDNA (Figure S6A. Related to Figure 7), expansion of Tem (Figure S6B. Related to Figure 7), CD4$^+$ICOS$^+$ (Figure S6C. Related to Figure 7), CD138$^+$ (Figure S6D. Related to Figure 7), germinal center B cells (Figure S6E. Related to Figure 7), and minimal immune complex deposition in the kidneys (Figures S6F–S6G. Related to Figure 7). Although only minimal IgG deposition was detected, these data suggested that STING-activated BMDC can induce autoimmunity. The background of WT recipient mice may not promote the overt phenotypes of autoimmune disease.

Next, we performed the reconstitution experiment by adoptive transfer of STING-activated BMDC into the double-deficient mice. The level of anti-dsDNA significantly increased in the mice receiving *Sting*-sufficient BMDC compared with those receiving *Sting*-deficient BMDC and control (Figure 7A). The transfer of BMDC in the double-deficient mice did not increase the expression of *Isg15*, *Mx1*, and *Irf7* (Figures 7B–7D); however, *Irf3* increased in the kidney of the recipient mice (Figure 7E).

The analysis of spleens showed an increase in the percentage of T_{em} and CD4$^+$ICOS$^+$ in recipient mice that received STING-activated BMDC derived from WT or *Fcgr2b*$^{-/-}$.*Sting*$^{wt/gt}$ mice when compared with the

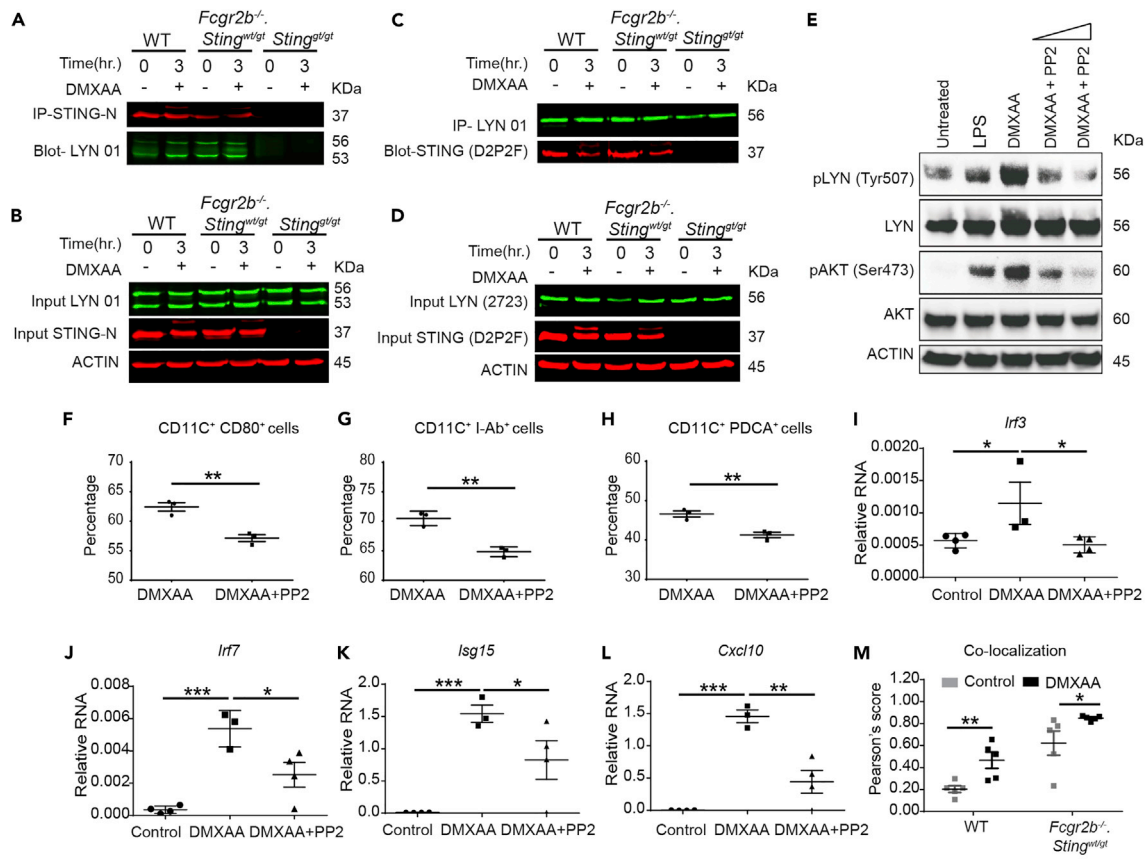
A
Fcgr2b-/-.
WT
Stingwt/gt
Stinggt/gt
Time(hr.)
0 3 0 3 0 3
DMXAA
- + - + - +
KDa
IP-STING-N
37
Blot- LYN 01
56
53
B
Input LYN 01
56
53
Input STING-N
37
ACTIN
45
C
IP- LYN 01
56
Blot-STING (D2P2F)
37
D
Input LYN (2723)
56
Input STING (D2P2F)
37
ACTIN
45
E
Untreated
LPS
DMXAA
DMXAA + PP2
DMXAA + PP2
KDa
pLYN (Tyr507)
56
LYN
56
pAKT (Ser473)
60
AKT
60
ACTIN
45
F
CD11C+ CD80+ cells
Percentage
DMXAA
DMXAA+PP2
G
CD11C+ I-Ab+ cells
H
CD11C+ PDCA+ cells
I
Irf3
Relative RNA
Control
DMXAA
DMXAA+PP2
J
Irf7
K
Isg15
L
Cxcl10
M
Co-localization
Control
DMXAA
Pearson's score
WT
Fcgr2b-/-.
Stingwt/gt
N
WT
Fcgr2b-/-.Stingwt/gt
Stinggt/gt
Control
DMXAA
DAPI
STING-C
LYN-Clone (2723)
Merge

Figure 6. STING Activation Induced DC Maturation and Promoted the Interaction between LYN and STING in DC

(A–D) Fluorescent western blot shows (A) the immunoprecipitation (IP) with STING-N (red) and blots with Lyn (green) and (B) cell lysate of activated BMDC with DMXAA at 0 and 3 h (C) A reverse IP using the Lyn antibody and blot with STING antibody and (D) cell lysate of activated BMDC with DMXAA at 0 and 3 h. Data show a representative of four experiments.

(E–L) (E) Western blot analysis of Sting-activated BMDC with or without PP2 inhibitor showed the phosphorylation of Lyn (Try507) and Akt (Ser473). Data are representative of three mice per group. Sting-activated BMDCs were cultured with Lyn inhibitor (PP2) and analyzed by (F–H) flow cytometry shows the percentage of (F) $CD80^+CD11c^+$, (G) $I\text{-}Ab^+CD11c^+$, and (H) $PDCA^+CD11c^+$ cells (N = 3 per group), and (I–L) the relative RNA expression (normalized by actin) of (I) *Irf3*, (J) *Irf7*, (K) Is*g15*, and (L) *Cxcl10* are shown (N = 4 per group).

(M and N) Confocal microscopy of DMXAA-activated BMDC from WT, $Sting^{gt/gt}$, and $Fcgr2b^{-/-}$. $Sting^{wt/gt}$ - mice for 6 h. (M) The quantification of colocalization signals between STING and Lyn (N = 5 per group). Data are shown as mean ± SEM; *p < 0.05, **p < 0.01, and ***p < 0.001. (N) Immunofluorescence staining of BMDC shows Lyn (green), STING (red), and DAPI (blue) (scale bar, 20 μm). Data show a representative of five experiments.

PBS control and double-deficient BMDC injection group (Figures 7F and 7G). These data suggested that T cell phenotypes required STING expression in BMDC. Interestingly, only *Sting*-sufficient BMDC from $Fcgr2b^{-/-}$, but not WT mice, induced the spontaneous germinal center B cell formation. Also, *Sting*-deficient BMDC from $Fcgr2b^{-/-}$ did not increase germinal center B cell (Figure 7H). Next, we examined the immunofluorescence staining to identify the immune complexes at the kidney of the recipient. The recipient of *Sting*-sufficient BMDC showed an increase of IgG deposition and $CD45^+$ cell infiltration, whereas *Sting*-deficient BMDC did not (Figures 7I–7N).

Nevertheless, the $Fcgr2b^{-/-}$ BMDC induced more immune complexes and $CD45^+$ cells in the kidneys (Figures 7J and 7K). The results suggested that the restoration of the STING signaling pathway in dendritic cells is essential for lupus development in the $Fcgr2b^{-/-}.Sting^{gt/gt}$ mice. The *Sting*-sufficient BMDC induced the lupus phenotypes in the double-deficient mice via the activation of T and B cells, which led to autoantibody production rather than promote type I IFN signaling.

DISCUSSION

A gain-of-function mutation in STING has been identified as a gene responsible for a subpopulation of patients with SLE, and STING-dependent interferon-inducible genes correlated with disease activity (Kato et al., 2018; Konig et al., 2017). However, there are no functional data of STING in a lupus mouse model that are relevant to human SLE. The 129/B6.$Fcgr2b^{-/-}$ mice carrying Nba2 region expressed constitutively *Ifi202*. The $CD19^+$ cells from B6.Nba2 show the increase of *Ifi202* and the decrease of *Sting* expression (Panchanathan et al., 2013). However, the overexpression of *Ifi202* can activate the Sting-dependent IFN-I response and the 129/B6.$Fcgr2b^{-/-}$ mice increase the expression of IFN-β (Brunette et al., 2012; Panchanathan et al., 2011). Here, we detected the high expression of *Sting*, *Ifn-β*, and interferon-inducible genes from the spleen of these mice. The activation of cGAS leads to cGAMP production and subsequently activates STING signaling (Sun et al., 2013; Wu et al., 2013). The increase of cGAMP in the 129/B6.$Fcgr2b^{-/-}$ mice raised the question of the natural origin of DNA that stimulates the cGAS-STING pathway. The $Fcgr2b^{-/-}$ mice showed the cGAMP overproduction, whereas the disruption of STING decreased the level of cGAMP in the $Fcgr2b^{-/-}$ mice. On the contrary to a previous study, the increase of cGAMP in *Trex1* and *DnaseII*-deficient mice was upregulated in the absence of STING (Gao et al., 2015). TREX1 degrades double-stranded DNA, whereas oxidized DNA is resistant to TREX1-mediated degradation (Gehrke et al., 2013; Grieves et al., 2015). Also, DNASE II cleaves native dsDNA but works less effectively for denaturized DNA (Laukova et al., 2020). Moreover, the mitochondrial DNA (mtDNA) releasing into the cytosol can trigger the IFN-I response and accelerates the severity of a mouse model of lupus disease (Kim et al., 2019). The mtDNA released into the cytosol activates the cGAS-STING pathway in cisplatin-induced tubular inflammation (Maekawa et al., 2019). Since the absence of STING reduced the level of cGAMP in the $Fcgr2b^{-/-}$ mice, but not in the $Trex1^{-/-}$ and $DnaseII^{-/-}$ mice, the intrinsic DNA origin that constitutively activates the STING-cGAS pathway should be different among these autoimmune mouse models. The $Fcgr2b^{-/-}.Sting^{gt/gt}$ mice did not develop overt kidney inflammation; thus, it is likely to release less amount of oxidized mtDNA. The cytosolic DNA that constitutively activates STING-cGAS pathway in the $Fcgr2b^{-/-}$ mice may originate from stress-induced mitochondrial DNA leakage from inflammation. These findings suggested that specific types of DNA from different compartments could be sensed and activated through the STING-cGAS pathway.

Although STING functions as a negative regulator in the Mrl/*lpr* lupus mice (Sharma et al., 2015), our data show that STING is required for the lupus development in the 129/B6.$Fcgr2b^{-/-}$ mice. STING may also play a crucial role in other lupus mouse models, which contained the Nba2 region. The survival of the 129/B6.$Fcgr2b^{-/-}$ mice

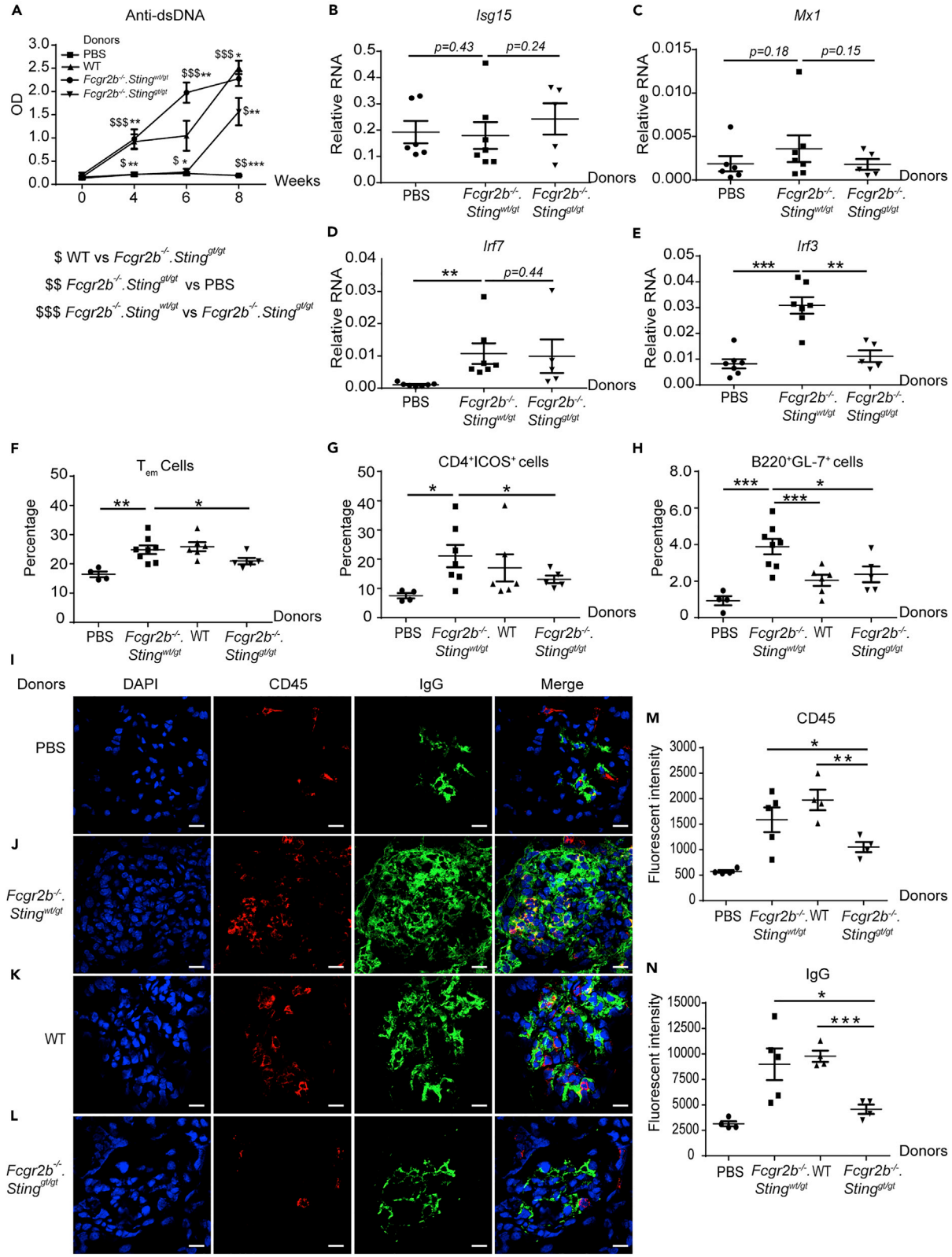
A
Anti-dsDNA
Donors
PBS
WT
Fcgr2b-/-.Stingwt/gt
Fcgr2b-/-.Stinggt/gt
OD
Weeks
$ WT vs Fcgr2b-/-.Stinggt/gt
$$ Fcgr2b-/-.Stinggt/gt vs PBS
$$$ Fcgr2b-/-.Stingwt/gt vs Fcgr2b-/-.Stinggt/gt
B
Isg15
Relative RNA
p=0.43
p=0.24
C
Mx1
p=0.18
p=0.15
D
Irf7
p=0.44
E
Irf3
F
Tem Cells
Percentage
G
CD4+ICOS+ cells
H
B220+GL-7+ cells
I
DAPI
CD45
IgG
Merge
PBS
J
Fcgr2b-/-.Stingwt/gt
K
WT
L
Fcgr2b-/-.Stinggt/gt
M
CD45
Fluorescent intensity
N
IgG

Figure 7. Adoptive Transfer of *Sting*-Expressing BMDC Induces Lupus Development in the *Fcgr2b*$^{-/-}$.*Sting* $^{gt/gt}$ Mice

DMXAA-activated BMDC from *Fcgr2b*$^{-/-}$.*Sting*$^{wt/gt}$, WT, and *Fcgr2b*$^{-/-}$.*Sting*$^{gt/gt}$ were transferred into the recipient mice (*Fcgr2b*$^{-/-}$.*Sting*$^{gt/gt}$).

(A) The level of anti-dsDNA from the sera (1:100) measured by ELISA (N = 5–10 per group). The dollar sign ($) shows the comparison between the groups.

(B–E) The relative RNA expressions (normalized by actin) of (B) *Isg15*, (C) *Mx1*, (D) *Irf7*, and (E) *Irf3* in the kidney of the mice receiving BMDC are shown (N = 5–6 per group).

(F–H) Flow cytometry analysis of recipient splenocytes after BMDC transferred every 2 weeks for four times shows the percentage of (F) T_{em} ($CD4^+CD44^{hi}CD62L^{lo}$), (G) $CD4^+ICOS^+$ cells, (H) $B220^+GL7^+$ cells (N = 5–10 per group).

(I–L) Immunofluorescence staining of the kidney from the *Fcgr2b*$^{-/-}$.*Sting*$^{gt/gt}$ recipient mice after the transfer with (I) PBS control, DMXAA-activated BMDC from (J) *Fcgr2b*$^{-/-}$.*Sting*$^{wt/gt}$, (K) WT, and (L) *Fcgr2b*$^{-/-}$.*Sting*$^{gt/gt}$. The confocal microscope shows DAPI (blue), CD45 (red), and IgG (green). The representative of four experiments (scale bar, 10 μm).

(M and N) The quantification of fluorescence intensity of (M) CD45, and (N) IgG staining.

Data are shown as mean ± SEM; *p < 0.05, **p < 0.01, and ***p < 0.001.

depend on autoantibody production and glomerulonephritis (Bolland et al., 2002; Pisitkun et al., 2012). STING is required for the antibody production induced by cyclic-di-GMP *in vitro* (Walker et al., 2018). These data suggested that STING facilitated the autoantibody production, inflammatory cell infiltration, and glomerulonephritis in the 129/B6.*Fcgr2b*$^{-/-}$ mice. The expression of interferon-inducible genes associated with SLE disease activity (Feng et al., 2006). We detected the very high expression of IFN-inducible genes in the kidneys of 129/B6.*Fcgr2b*$^{-/-}$ mice showed severe pathology. The absence of STING signaling in the *Fcgr2b*$^{-/-}$ mice partly decreased the expression of interferon-inducible genes in the kidney. The kidneys in the experiment were not perfused; thus, we cannot conclude that the IFN signature expressed in the kidney derived from the blood or kidney. These data suggested that other nucleic acid sensors may promote the type I interferon production or signaling in the *Fcgr2b*$^{-/-}$ mice as well, and STING-dependent lupus phenotypes do not mediate only through type-I interferon pathway.

STING expresses and functions differentially depending on the cell types. STING signals synergistically with B cell receptor signaling to promote antibody response (Walker et al., 2018). Our results showed that spontaneous germinal center B cells and MHC-II expression in the *Fcgr2b*$^{-/-}$ mice were *Sting* dependent. However, plasma cell expansion was *Sting* independent. These data suggested STING may contribute to the autoantibody production through memory B cells. STING also activates T cells, which induced type I IFN production and mediated cell death (Larkin et al., 2017). Nevertheless, we found that the increase of T effector memory (T_{em}) in the *Fcgr2b*$^{-/-}$ mice was *Sting* dependent. The expansion of T_{em} may directly mediate through the interaction with antigen-presenting cells, not via Sting signaling in T cells.

STING agonist (DMXAA)-treated mice show the increased expression of CD80, CD86, and MHC-II on DC, suggesting the mature phenotypes of DC as the antigen-presenting cells (APCs) (Curran et al., 2016). We observed the reduction of DC expansion in the *Fcgr2b*$^{-/-}$ mice, which depended on STING signaling. We confirmed that STING was required for DC maturation and cytokine production. These DCs became professional APCs and could promote T cell differentiation. The IFN-γ-producing $CD4^+$ cells in the spleen of the *Fcgr2b*$^{-/-}$ mice were reduced in the absence of STING. The *Sting*-expressing DCs derived from WT and *Fcgr2b*$^{-/-}$ mice stimulated naive T cells to proliferate; however, the ability of T cells to differentiate and produce IFN-γ did not depend on intrinsic *Sting* expression on T cells. Interestingly, only DCs from the *Fcgr2b*$^{-/-}$ mice can increase the IFN-γ production in $CD4^+$ T cells. These data suggested the DC from the *Fcgr2b*$^{-/-}$ mice have the intrinsic property that promotes the generation of IFN-γ-producing $CD4^+$ T cells.

The cGAS-STING signaling can activate human pDCs to produce IFN-I, and knockdown of *Sting* using siRNA in CAL-1 cells can cause the reduction of IFN response (Bode et al., 2016). The proteomic data showed the upregulation of interferon-regulated protein after STING activation with DMXAA, which implied that the culture environment should enrich with type-I IFN. STING activation led to phosphorylation of Ser357 of mouse Sting (homolog Ser358 in human Sting), and this site is phosphorylated by TBK1 which subsequently promoting type I IFN production (Tanaka and Chen, 2012; Zhong et al., 2008). The identification of pDC after STING activation uncovered the role of STING in the differentiation of pDC. These data revealed that STING was essential for the generation of pDCs. Besides, our study identified several STING-interacting proteins by mass spectrometry. Lyn kinase has been shown to have role in the differentiation of pDC (Dallari et al., 2017). The recruitment of LYN to STING after DMXAA stimulation suggested STING-mediated signaling through Lyn kinase. Also, the proteomics data of STING-activated BMDC showed a significant increase of phosphoinositide 3-kinase adapter protein 1 (Pik3ap1) and receptor of activated protein C kinase 1 (Rack1) (Table S1. Lists of up- and down-regulated proteins. Related to

Figure 5). Pik3ap1 is an adaptor that signals to the phosphoinositide 3-kinase (PI3K) (Aiba et al., 2008). LYN and RACK1 are co-immunoprecipitated in membrane complexes (Sutton et al., 2013). Also, RACK1 silencing affected the phosphorylation of AKT (Liu et al., 2017). Our data suggest that the downstream of STING-LYN signaling mediated through the PI3K-AKT pathway. The inhibition of Lyn kinase with PP2 inhibitor during STING activation diminished DC maturation and pDC differentiation. The PP2 also is a broad inhibitor of other Src kinase family. However, we could identify the interaction of LYN and STING by mass spectrometry, immunoprecipitation, and colocalization during STING activation. All of these data suggested STING-mediated differentiation of BMDC probably through the LYN signaling pathway.

The duration of the transfer experiment was 8 weeks. Thus, the phenotypes that have changed would not be apparent lupus, but still, the hallmarks of lupus disease settled down in the recipient mice. However, the increase of anti-dsDNA in the serum, immune complex deposition, and inflammatory cell infiltration in the kidney were detected in the recipient mice when transferring the STING-sufficient BMDC into the double-deficient recipient mice.

The depletion of pDC ameliorates the autoimmune phenotypes in BXSB lupus-prone mice and B6.Nba2 mice (Davison and Jørgensen, 2015; Rowland et al., 2014). Our data strongly suggested STING involving in DC function both DC maturation and pDC differentiation. Adoptive transfer of *Sting*-sufficient BMDCs can induce autoantibody production and immune complex deposition regardless of the *Fcgr2b* status. However, the absence of *Fcg2b* in the BMDC can accelerate the severity of autoimmune phenotypes and notably increase inflammatory cell infiltration in the kidney of the double-deficient recipient mice.

The transfer of *Sting*-sufficient *Fcgr2b*$^{-/-}$ BMDC led to an increase of *Irf3* expression but not *Isg15, Mx1, and Irf7*. Irf3 is a transcription factor downstream of STING signaling pathway (Burdette et al., 2011). These data suggested that *Irf3* expression in the kidney was STING-dependent BMDC, whereas other ISGs may depend on the intrinsic STING expression of the resident cells in the kidney. Besides, the transfer of *Sting*-sufficient *Fcgr2b*$^{-/-}$BMDC could increase the effector T cell and germinal center B cells in the spleens of the recipient mice. These data suggested that STING expression on BMDC is essential for the initiation of autoimmunity in the double-deficient mice via the activation of T and B cells, which led to autoantibody production rather than the promotion of type I IFN signaling.

In summary, this study established the vital function of STING in the autoimmune *Fcgr2b*$^{-/-}$ lupus mouse model, thus providing a reliable tool for future mechanistic and preclinical studies of STING in SLE. These findings provide proof of the concept that inhibition of STING signaling may be a candidate targeted treatment for a subset of patients with SLE.

Limitations of the Study

This study identified the functional role of LYN in the differentiation of BMDC based on the PP2 inhibitor, which is a broad inhibitor for the Src kinase family. The *Lyn*-deficient BMDC will be solid proof to conclude that STING mediated DC differentiation via LYN kinase. However, the identification of LYN that immunoprecipitated with STING in BMDC by mass spectrometry but not other members of the Src family suggested the interaction of LYN and STING in the BMDC. Furthermore, we showed the vital role of STING in the *Fcgr2b*-deficient mice, one of the lupus mice models. The study of STING function in the human SLE in the future research would suggest the promising target to inhibit STING signaling in the treatment of SLE.

Resource Availability

Lead Contact

Further information and requests for resources and reagents should be directed to the Lead Contact, Dr. Prapaporn Pisitkun (Prapaporn.pis@mahidol.ac.th).

Materials Availability

Materials are available from the corresponding author on a reasonable request.

Data and Code Availability

The microarray data are available at Gene Expression Omnibus: GSE142594 and https://www.ncbi.nlm.nih.gov/geo/query/acc.cgi?acc=GSE142594.

The mass spectrometry proteomics data have been deposited to the ProteomeXchange Consortium via the PRoteomics IDEntifications (PRIDE) partner repository with the dataset identifier PXD019239.

METHODS

All methods can be found in the accompanying Transparent Methods supplemental file.

SUPPLEMENTAL INFORMATION

Supplemental Information can be found online at https://doi.org/10.1016/j.isci.2020.101530.

ACKNOWLEDGMENTS

This work was supported by the Thailand Research Fund (TRF), Thailand, RSA5980023 to P.P., International Network for Lupus Research (IRN59W0004) from TRF, Thailand, to P.P., T.P., and P.W., the National Research Council of Thailand (NRCT), Thailand, to Chulalongkorn University (2015-2018) and Chulalongkorn University, Thailand, GB-CU-61-25-30-15 to T.P. and P.P., and Chulalongkorn Academic Advancement into the 2nd Century (CUAASC) Project to T.P. T.P. was supported by Thailand Research Fund (TRF), Thailand, for Research Career Development Grant (RSA6280026). J.M. was supported by TRF, International Network for Lupus Research, Thailand, (IRN59W0004).

AUTHOR CONTRIBUTIONS

A.T. performed experiments, interpreted data, co-directed the study, and wrote the manuscript. T. Prabakaran performed and analyzed the *in vitro* functional assays with inhibitor. M.T. and T.B. provided experimental assistance for flow cytometry. J.M. performed the proteomics analysis. P.W. provided experimental assistance for mass spectrometry. N.C. provided experimental support for confocal microscopy. T.S. provided analysis assistance for microarray. A.L. analyzed and scored histopathology of tissue sections. S.P. provided reagents and expertise related to Sting signaling, co-directed the study, and edited the manuscript. T Pisitkun contributed reagents and expertise related to mass spectrometry, co-directed the study, and edited the manuscript. P.P. performed experiments, interpreted data, directed the studies, and wrote the manuscript.

DECLARATION OF INTERESTS

The authors declare no conflict of interest.

Received: December 19, 2019
Revised: May 15, 2020
Accepted: September 1, 2020
Published: September 25, 2020

REFERENCES

Ahn, J., Gutman, D., Saijo, S., and Barber, G.N. (2012). STING manifests self DNA-dependent inflammatory disease. Proc. Natl. Acad. Sci. U S A *109*, 19386–19391.

Ahn, J., Ruiz, P., and Barber, G.N. (2014). Intrinsic self-DNA triggers inflammatory disease dependent on STING. J. Immunol. *193*, 4634–4642.

Aiba, Y., Kameyama, M., Yamazaki, T., Tedder, T.F., and Kurosaki, T. (2008). Regulation of B-cell development by BCAP and CD19 through their binding to phosphoinositide 3-kinase. Blood *111*, 1497.

An, J., Durcan, L., Karr, R.M., Briggs, T.A., Rice, G.I., Teal, T.H., Woodward, J.J., and Elkon, K.B. (2017). Expression of cyclic GMP-AMP synthase in patients with systemic lupus erythematosus. Arthritis Rheum. *69*, 800–807.

Asselin-Paturel, C., Brizard, G., Chemin, K., Boonstra, A., O'Garra, A., Vicari, A., and Trinchieri, G. (2005). Type I interferon dependence of plasmacytoid dendritic cell activation and migration. J. Exp. Med. *201*, 1157–1167.

Baechler, E.C., Batliwalla, F.M., Karypis, G., Gaffney, P.M., Ortmann, W.A., Espe, K.J., Shark, K.B., Grande, W.J., Hughes, K.M., Kapur, V., et al. (2003). Interferon-inducible gene expression signature in peripheral blood cells of patients with severe lupus. Proc. Natl. Acad. Sci. U S A *100*, 2610–2615.

Bode, C., Fox, M., Tewary, P., Steinhagen, A., Ellerkmann, R.K., Klinman, D., Baumgarten, G., Hornung, V., and Steinhagen, F. (2016). Human plasmacytoid dentritic cells elicit a Type I Interferon response by sensing DNA via the cGAS-STING signaling pathway. Eur. J. Immunol. *46*, 1615–1621.

Bolland, S., and Ravetch, J.V. (2000). Spontaneous autoimmune disease in FcγRIIB-deficient mice results from strain-specific epistasis. Immunity *13*, 277–285.

Bolland, S., Yim, Y.-S., Tus, K., Wakeland, E.K., and Ravetch, J.V. (2002). Genetic modifiers of systemic lupus erythematosus in FcγRIIB−/− mice. J. Exp. Med. *195*, 1167–1174.

Boross, P., Arandhara, V.L., Martin-Ramirez, J., Santiago-Raber, M.-L., Carlucci, F., Flierman, R., van der Kaa, J., Breukel, C., Claassens, J.W.C., Camps, M., et al. (2011). The inhibiting Fc receptor for IgG, FcγRIIB, is a modifier of autoimmune susceptibility. J. Immunol. *187*, 1304.

Brunette, R.L., Young, J.M., Whitley, D.G., Brodsky, I.E., Malik, H.S., and Stetson, D.B. (2012). Extensive evolutionary and functional diversity among mammalian AIM2-like receptors. J. Exp. Med. *209*, 1969–1983.

Burdette, D.L., Monroe, K.M., Sotelo-Troha, K., Iwig, J.S., Eckert, B., Hyodo, M., Hayakawa, Y.,

and Vance, R.E. (2011). STING is a direct innate immune sensor of cyclic di-GMP. Nature *478*, 515–518.

Choubey, D. (2012). Interferon-inducible Ifi200-family genes as modifiers of lupus susceptibility. Immunol. Lett. *147*, 10–17.

Choubey, D., and Panchanathan, R. (2008). Interferon-inducible Ifi200-family genes in systemic lupus erythematosus. Immunol. Lett. *119*, 32–41.

Christensen, S.R., Shupe, J., Nickerson, K., Kashgarian, M., Flavell, Richard A., and Shlomchik, M.J. (2006). Toll-like receptor 7 and TLR9 dictate autoantibody specificity and have opposing inflammatory and regulatory roles in a murine model of lupus. Immunity *25*, 417–428.

Chu, C.-L., and Lowell, C.A. (2005). The Lyn tyrosine kinase differentially regulates dendritic cell generation and maturation. J. Immunol. *175*, 2880.

Crow, Y.J., Hayward, B.E., Parmar, R., Robins, P., Leitch, A., Ali, M., Black, D.N., van Bokhoven, H., Brunner, H.G., Hamel, B.C., et al. (2006). Mutations in the gene encoding the 3′-5′ DNA exonuclease TREX1 cause Aicardi-Goutières syndrome at the AGS1 locus. Nat. Genet. *38*, 917–920.

Curran, E., Chen, X., Corrales, L., Kline, D.E., Dubensky, T.W., Jr., Duttagupta, P., Kortylewski, M., and Kline, J. (2016). STING pathway activation stimulates potent immunity against acute myeloid leukemia. Cell Rep. *15*, 2357–2366.

Dallari, S., Macal, M., Loureiro, M.E., Jo, Y., Swanson, L., Hesser, C., Ghosh, P., and Zuniga, E.I. (2017). Src family kinases Fyn and Lyn are constitutively activated and mediate plasmacytoid dendritic cell responses. Nat. Commun. *8*, 14830.

Davison, L.M., and Jørgensen, T.N. (2015). Sialic acid–binding immunoglobulin-type lectin H–positive plasmacytoid dendritic cells drive spontaneous lupus-like disease development in B6.Nba2 mice. Arthritis Rheumatol. *67*, 1012–1022.

Deane, J.A., Pisitkun, P., Barrett, R.S., Feigenbaum, L., Town, T., Ward, J.M., Flavell, R.A., and Bolland, S. (2007). Control of toll-like receptor 7 expression is essential to restrict autoimmunity and dendritic cell proliferation. Immunity *27*, 801–810.

Feng, X., Wu, H., Grossman, J.M., Hanvivadhanakul, P., FitzGerald, J.D., Park, G.S., Dong, X., Chen, W., Kim, M.H., Weng, H.H., et al. (2006). Association of increased interferon-inducible gene expression with disease activity and lupus nephritis in patients with systemic lupus erythematosus. Arthritis Rheum. *54*, 2951–2962.

Gao, D., Li, T., Li, X.D., Chen, X., Li, Q.Z., Wight-Carter, M., and Chen, Z.J. (2015). Activation of cyclic GMP-AMP synthase by self-DNA causes autoimmune diseases. Proc. Natl. Acad. Sci. U S A *112*, E5699–E5705.

Gehrke, N., Mertens, C., Zillinger, T., Wenzel, J., Bald, T., Zahn, S., Tuting, T., Hartmann, G., and Barchet, W. (2013). Oxidative damage of DNA confers resistance to cytosolic nuclease TREX1 degradation and potentiates STING-dependent immune sensing. Immunity *39*, 482–495.

Grieves, J.L., Fye, J.M., Harvey, S., Grayson, J.M., Hollis, T., and Perrino, F.W. (2015). Exonuclease TREX1 degrades double-stranded DNA to prevent spontaneous lupus-like inflammatory disease. Proc. Natl. Acad. Sci. U S A *112*, 5117–5122.

Günther, C., Hillebrand, M., Brunk, J., and Lee-Kirsch, M.A. (2013). Systemic involvement in TREX1-associated familial chilblain lupus. J. Am. Acad. Dermatol. *69*, e179–e181.

Hron, J.D., and Peng, S.L. (2004). Type I IFN protects against murine lupus. J. Immunol. *173*, 2134.

Ishikawa, H., Ma, Z., and Barber, G.N. (2009). STING regulates intracellular DNA-mediated, type I interferon-dependent innate immunity. Nature *461*, 788.

Kato, Y., Park, J., Takamatsu, H., Konaka, H., Aoki, W., Aburaya, S., Ueda, M., Nishide, M., Koyama, S., Hayama, Y., et al. (2018). Apoptosis-derived membrane vesicles drive the cGAS-STING pathway and enhance type I IFN production in systemic lupus erythematosus. Ann. Rheum. Dis. *77*, 1507–1515.

Keating, S.E., Baran, M., and Bowie, A.G. (2011). Cytosolic DNA sensors regulating type I interferon induction. Trends Immunol. *32*, 574–581.

Kim, J., Gupta, R., Blanco, L.P., Yang, S., Shteinfer-Kuzmine, A., Wang, K., Zhu, J., Yoon, H.E., Wang, X., Kerkhofs, M., et al. (2019). VDAC oligomers form mitochondrial pores to release mtDNA fragments and promote lupus-like disease. Science *366*, 1531–1536.

Kimkong, I., Avihingsanon, Y., and Hirankarn, N. (2010). Association of IFI200 gene polymorphisms with susceptibility to systemic lupus erythematosus. J. Rheumatol. *37*, 1544–1547.

Konig, N., Fiehn, C., Wolf, C., Schuster, M., Cura Costa, E., Tungler, V., Alvarez, H.A., Chara, O., Engel, K., Goldbach-Mansky, R., et al. (2017). Familial chilblain lupus due to a gain-of-function mutation in STING. Ann. Rheum. Dis. *76*, 468–472.

Larkin, B., Ilyukha, V., Sorokin, M., Buzdin, A., Vannier, E., and Poltorak, A. (2017). Cutting edge: activation of STING in T cells induces type I IFN responses and cell death. J. Immunol. *199*, 397–402.

Laukova, L., Konecna, B., Janovicova, L., Vlkova, B., and Celec, P. (2020). Deoxyribonucleases and their applications in biomedicine. Biomolecules *10*, 1036.

Liu, B., Wang, C., Chen, P., Wang, L., and Cheng, Y. (2017). RACK1 promotes radiation resistance in esophageal cancer via regulating AKT pathway and Bcl-2 expression. Biochem. Biophysical Res. Commun. *491*, 622–628.

Maekawa, H., Inoue, T., Ouchi, H., Jao, T.M., Inoue, R., Nishi, H., Fujii, R., Ishidate, F., Tanaka, T., Tanaka, Y., et al. (2019). Mitochondrial damage causes inflammation via cGAS-STING signaling in acute kidney injury. Cell Rep. *29*, 1261–1273 e1266.

Marinho, F.V., Benmerzoug, S., Rose, S., Campos, P.C., Marques, J.T., Báfica, A., Barber, G., Ryffel, B., Oliveira, S.C., and Quesniaux, V.F.J. (2018). The cGAS/STING pathway is important for dendritic cell activation but is not essential to induce protective immunity against *Mycobacterium tuberculosis* infection. J. Innate Immun. *10*, 239–252.

Morita, M., Stamp, G., Robins, P., Dulic, A., Rosewell, I., Hrivnak, G., Daly, G., Lindahl, T., and Barnes, D.E. (2004). Gene-targeted mice lacking the Trex1 (DNase III) 3′–>5′ DNA exonuclease develop inflammatory myocarditis. Mol. Cell. Biol. *24*, 6719–6727.

Murphy, E.D., and Roths, J.B. (1979). A y chromosome associated factor in strain bxsb producing accelerated autoimmunity and lymphoproliferation. Arthritis Rheum. *22*, 1188–1194.

Muskardin, T.L.W., and Niewold, T.B. (2018). Type I interferon in rheumatic diseases. Nat. Rev. Rheumatol. *14*, 214–228.

Nickerson, K.M., Christensen, S.R., Shupe, J., Kashgarian, M., Kim, D., Elkon, K., and Shlomchik, M.J. (2010). TLR9 regulates TLR7- and MyD88-dependent autoantibody production and disease in a murine model of lupus. J. Immunol. *184*, 1840.

Paludan, S.R. (2015). Activation and regulation of DNA-driven immune responses. Microbiol. Mol. Biol. Rev. *79*, 225.

Panchanathan, R., Liu, H., Xin, D., and Choubey, D. (2013). Identification of a negative feedback loop between cyclic di-GMP-induced levels of IFI16 and p202 cytosolic DNA sensors and STING. Innate Immun. *20*, 751–759.

Panchanathan, R., Shen, H., Duan, X., Rathinam, V.A.K., Erickson, L.D., Fitzgerald, K.A., and Choubey, D. (2011). Aim2 deficiency in mice suppresses the expression of the inhibitory Fcgamma receptor (FcgammaRIIB) through the induction of the IFN-inducible p202, a lupus susceptibility protein. J. Immunol. *186*, 6762–6770.

Pisitkun, P., Deane, J.A., Difilippantonio, M.J., Tarasenko, T., Satterthwaite, A.B., and Bolland, S. (2006). Autoreactive B cell responses to RNA-related antigens due to TLR7 gene duplication. Science *312*, 1669.

Pisitkun, P., Ha, H.-L., Wang, H., Claudio, E., Tivy, C.C., Zhou, H., Mayadas, T.N., Illei, G.G., and Siebenlist, U. (2012). Interleukin-17 cytokines are critical in development of fatal lupus glomerulonephritis. Immunity *37*, 1104–1115.

Rowland, S.L., Riggs, J.M., Gilfillan, S., Bugatti, M., Vermi, W., Kolbeck, R., Unanue, E.R., Sanjuan, M.A., and Colonna, M. (2014). Early, transient depletion of plasmacytoid dendritic cells ameliorates autoimmunity in a lupus model. J. Exp. Med. *211*, 1977–1991.

Rozzo, S.J., Allard, J.D., Choubey, D., Vyse, T.J., Izui, S., Peltz, G., and Kotzin, B.L. (2001). Evidence for an interferon-inducible gene, Ifi202, in the susceptibility to systemic lupus. Immunity *15*, 435–443.

Sacre, K., Criswell, L.A., and McCune, J.M. (2012). Hydroxychloroquine is associated with impaired interferon-alpha and tumor necrosis factor-alpha

production by plasmacytoid dendritic cells in systemic lupus erythematosus. Arthritis Res. Ther. *14*, R155.

Sato-Hayashizaki, A., Ohtsuji, M., Lin, Q., Hou, R., Ohtsuji, N., Nishikawa, K., Tsurui, H., Sudo, K., Ono, M., Izui, S., et al. (2011). Presumptive role of 129 strain–derived Sle16 locus in rheumatoid arthritis in a new mouse model with Fcγ receptor type IIb–deficient C57BL/6 genetic background. Arthritis Rheum. *63*, 2930–2938.

Sauer, J.-D., Sotelo-Troha, K., von Moltke, J., Monroe, K.M., Rae, C.S., Brubaker, S.W., Hyodo, M., Hayakawa, Y., Woodward, J.J., Portnoy, D.A., and Vance, R.E. (2011). The N-ethyl-N-nitrosourea-induced Goldenticket mouse mutant reveals an essential function of Sting in the in vivo interferon response to Listeria monocytogenes and cyclic dinucleotides. Infect. Immun. *79*, 688–694.

Sharma, S., Campbell, A.M., Chan, J., Schattgen, S.A., Orlowski, G.M., Nayar, R., Huyler, A.H., Nündel, K., Mohan, C., Berg, L.J., et al. (2015). Suppression of systemic autoimmunity by the innate immune adaptor STING. Proc. Natl. Acad. Sci. U S A *112*, E710–E717.

Stetson, D.B., Ko, J.S., Heidmann, T., and Medzhitov, R. (2008). Trex1 prevents cell-intrinsic initiation of autoimmunity. Cell *134*, 587–598.

Sun, L., Wu, J., Du, F., Chen, X., and Chen, Z.J. (2013). Cyclic GMP-AMP synthase is a cytosolic DNA sensor that activates the type I interferon pathway. Science *339*, 786–791.

Sutton, P., Borgia, J.A., Bonomi, P., and Plate, J.M.D. (2013). Lyn, a Src family kinase, regulates activation of epidermal growth factor receptors in lung adenocarcinoma cells. Mol. Cancer *12*, 76.

Tanaka, Y., and Chen, Z.J. (2012). STING specifies IRF3 phosphorylation by TBK1 in the cytosolic DNA signaling pathway. Sci. Signal. *5*, ra20.

Theofilopoulos, A.N., and Dixon, F.J. (1985). Murine models of systemic lupus erythematosus. In Advances in Immunology, F.J. Dixon, ed. (Elsevier), pp. 269–390.

Unterholzner, L., Keating, S.E., Baran, M., Horan, K.A., Jensen, S.B., Sharma, S., Sirois, C.M., Jin, T., Latz, E., Xiao, T.S., et al. (2010). IFI16 is an innate immune sensor for intracellular DNA. Nat. Immunol. *11*, 997.

Walker, M.M., Crute, B.W., Cambier, J.C., and Getahun, A. (2018). B cell–intrinsic STING signaling triggers cell activation, synergizes with B cell receptor signals, and promotes antibody responses. J. Immunol. *201*, 2641.

Wu, J., Sun, L., Chen, X., Du, F., Shi, H., Chen, C., and Chen, Z.J. (2013). Cyclic GMP-AMP is an endogenous second messenger in innate immune signaling by cytosolic DNA. Science *339*, 826–830.

Yan, N. (2017). Immune diseases associated with TREX1 and STING dysfunction. J. Interferon Cytokine Res. *37*, 198–206.

Zeidi, M., Kim, H.J., and Werth, V.P. (2019). Increased myeloid dendritic cells and TNF-α expression predicts poor response to hydroxychloroquine in cutaneous lupus erythematosus. J. Invest. Dermatol. *139*, 324–332.

Zhong, B., Yang, Y., Li, S., Wang, Y.-Y., Li, Y., Diao, F., Lei, C., He, X., Zhang, L., Tien, P., and Shu, H.-B. (2008). The adaptor protein MITA links virus-sensing receptors to IRF3 transcription factor activation. Immunity *29*, 538–550.

Zhu, X.W., Wang, Y., Wei, Y.H., Zhao, P.P., Wang, X.B., Rong, J.J., Zhong, W.Y., Zhang, X.W., Wang, L., and Zheng, H.F. (2016). Comprehensive assessment of the association between FCGRs polymorphisms and the risk of systemic lupus erythematosus: evidence from a Meta-Analysis. Sci. Rep. *6*, 31617.

iScience, Volume *23*

Supplemental Information

STING Mediates Lupus via the Activation of Conventional Dendritic Cell Maturation and Plasmacytoid Dendritic Cell Differentiation

Arthid Thim-uam, Thaneas Prabakaran, Mookmanee Tansakul, Jiradej Makjaroen, Piriya Wongkongkathep, Naphat Chantaravisoot, Thammakorn Saethang, Asada Leelahavanichkul, Thitima Benjachat, Søren Paludan, Trairak Pisitkun, and Prapaporn Pisitkun

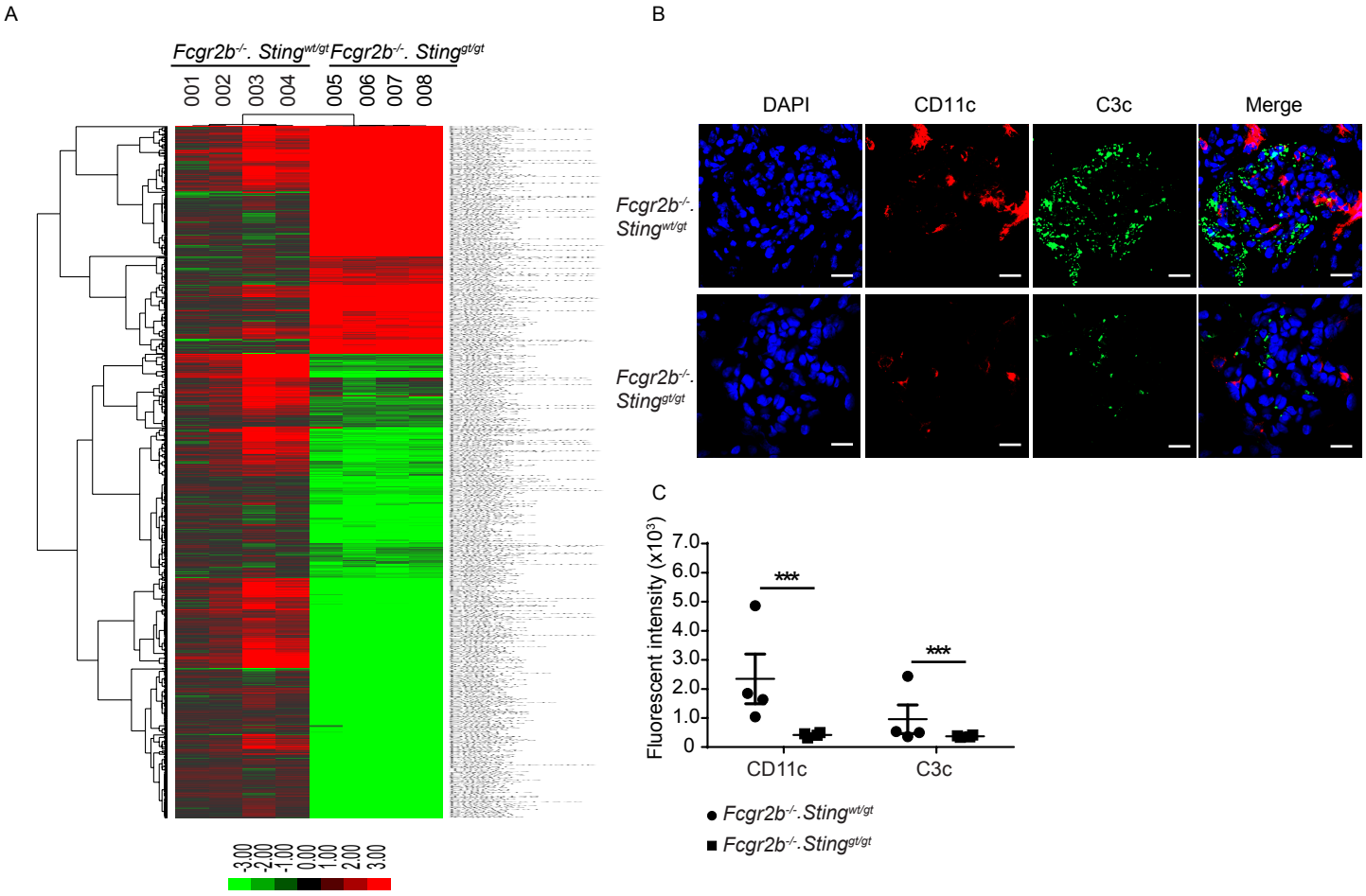

Figure S1. Phenotypes of kidney in the Fcgr2b$^{-/-}$. Sting$^{wt/gt}$ and Fcgr2b$^{-/-}$. Sting$^{gt/gt}$ mice at the age of 6-8 months, Related to Figure 2.
(A) Genes expression profiles of kidneys in the *Fcgr2b$^{-/-}$. Sting$^{wt/gt}$* and *Fcgr2b$^{-/-}$. Sting$^{gt/gt}$* mice. A heat map of microarray data shows the genes that significantly changed up to 2 fold compared between *Fcgr2b$^{-/-}$. Sting$^{wt/gt}$* and *Fcgr2b$^{-/-}$. Sting$^{gt/gt}$* mice (N=4 mice per group; $p<0.05$). Data show in log2 (sample/wild-type). (B) Immunofluorescence staining of the kidneys from *Fcgr2b$^{-/-}$. Sting$^{wt/gt}$* and *Fcgr2b$^{-/-}$. Sting$^{gt/gt}$* mice shows C3c (green), CD11c (red), and DAPI (blue). Data are representative of 4 mice per group (scale bar=10 μm). (C) The quantification of fluorescence intensity of CD11c and C3c was analyzed by ZEISS ZEN Microscope Software (Carl Zeiss, Germany) (N=4 mice per group). Data show as mean ± SEM; *$p < 0.05$, **$p<0.01$ and ***$p<0.001.1$).

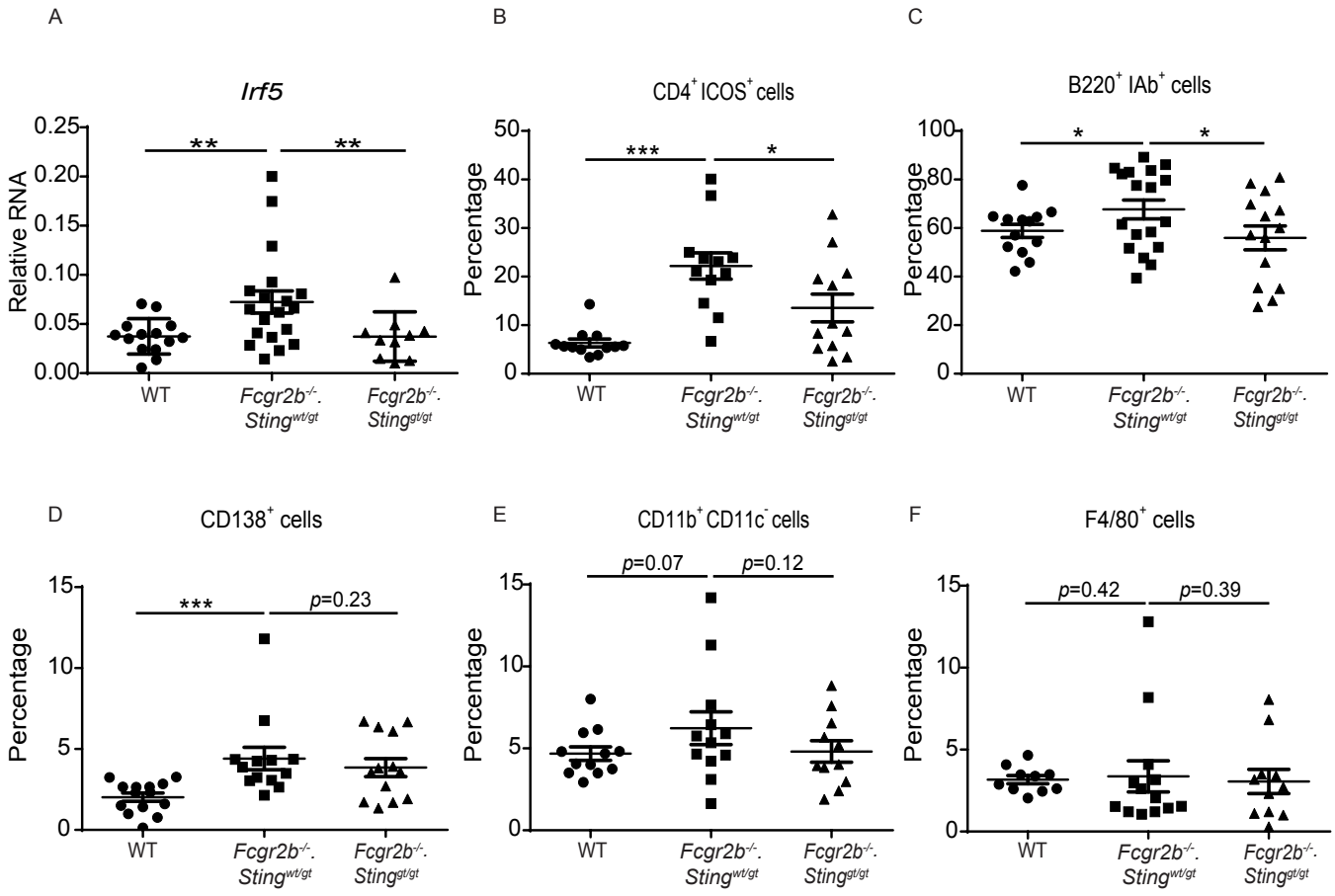

Figure S2. STING signaling is essential for immuno-phenotypes of the Fcgr2b$^{-/-}$. Sting$^{wt/gt}$ lupus mice,Related to Figure 3. (A) Gene expression from the kidneys of WT, *Fcgr2b$^{-/-}$. Sting$^{wt/gt}$* and *Fcgr2b$^{-/-}$. Sting$^{gt/gt}$* mice at the age of 6 months were tested by real-time PCR. The relative RNA (normalized by actin) of (A) *Irf5* is shown (N=10-17 per group). (B-F) Flow cytometry analysis of splenocytes isolated from WT, *Fcgr2b$^{-/-}$. Sting$^{wt/gt}$* and *Fcgr2b$^{-/-}$. Sting$^{gt/gt}$* mice at the age of 6-7 months (N= 13-14 per group). Data shown in the percentage of (B) CD4^{+} ICOS^{+} cells, (C) B220^{+} I-Ab^{+} cells, (D) CD138^{+} cells, (E) CD11b^{+} CD11c^{-} cells and (F) F4/80^{+} cells. Data show as mean ± SEM (*p < 0.05, **p<0.01 and ***p<0.001).

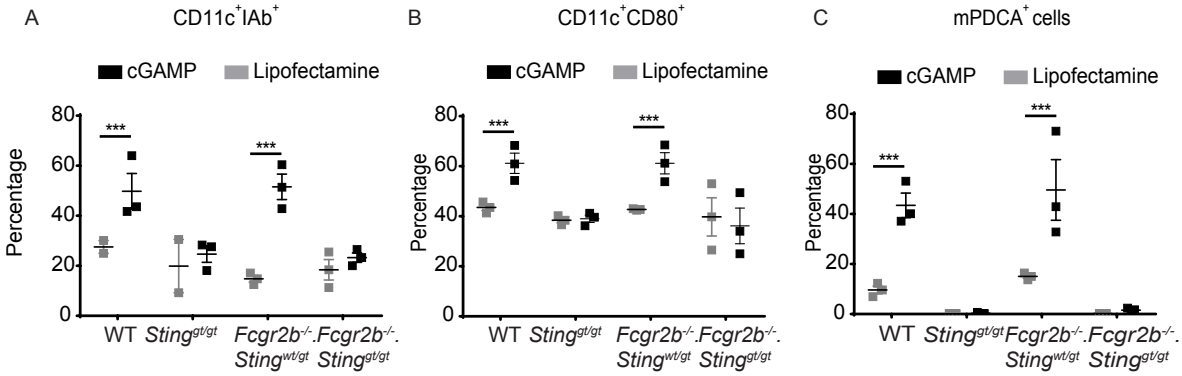

Figure S3. STING activation promotes the maturation of dendritic cells and the differentiation of plasmacytoid dendritic cells, Related to Figure 5. Bone marrows were isolated from WT, Sting$^{gt/gt}$, Fcgr2b$^{-/-}$. Sting$^{wt/gt}$ and Fcgr2b$^{-/-}$. Sting$^{gt/gt}$ mice atthe age of 6 months. (A-C) Bone marrow-derived dendritic cells were differentiated with IL-4 and GM-CSF differentiated for five days and subsequently stimulated with cGAMP for 24 hours. Flow cytometry analysis shows the percentage of (A) CD11c^{+} IAb^{+} cells and (B) CD11c^{+}CD80^{+} cells, and (C) PDCA^{+} cells after cGAMP activation (N=3). Data show as mean ± SEM; *p < 0.05, **p<0.01 and ***p<0.001.

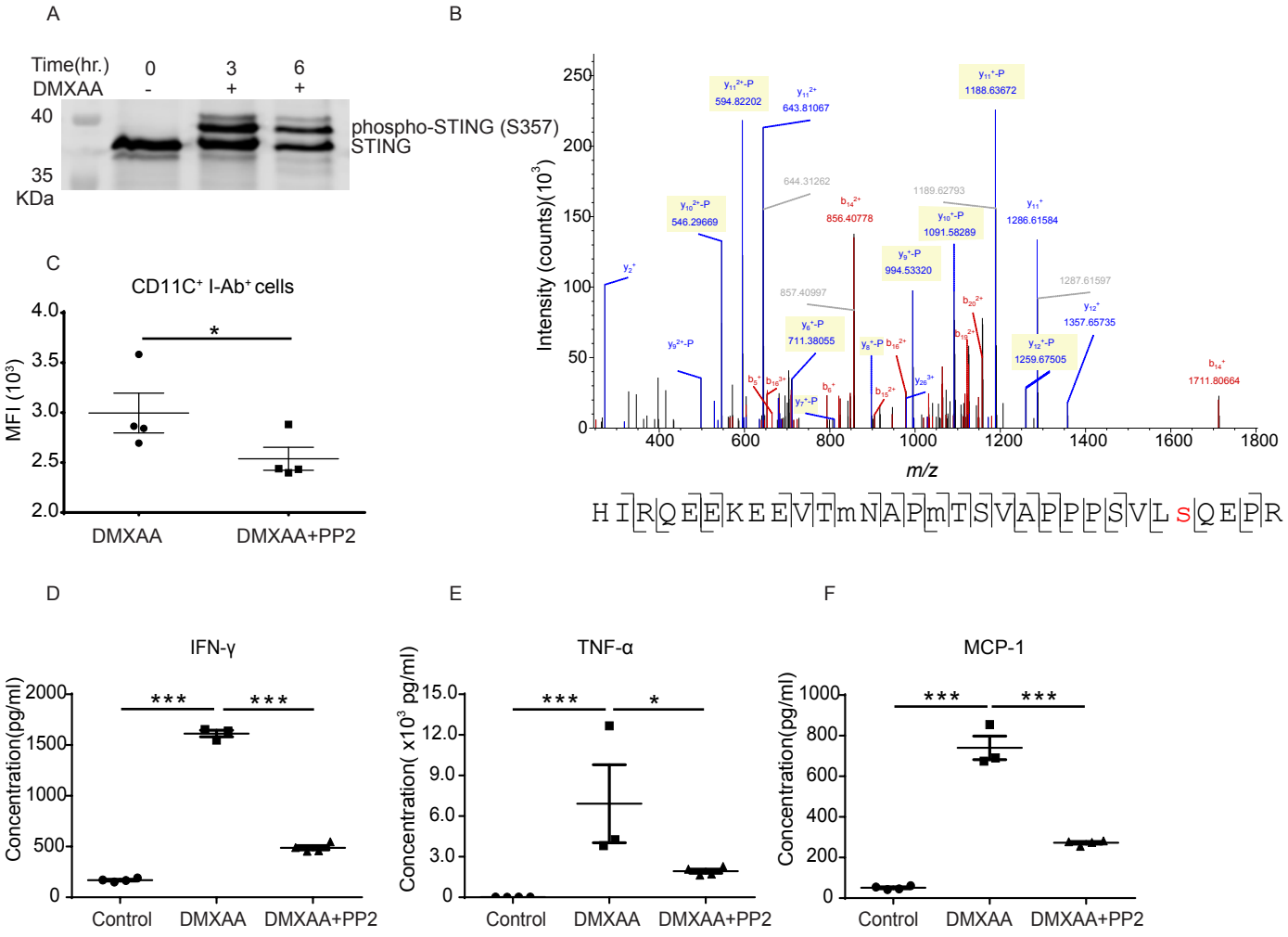

Figure S4. Phenotypes of STING activated dendritic cells, Related to Figure 6. (A) Representative of western blot analysis from immunoprecipitation with STING of *Fcgr2b*$^{-/-}$. *Sting*$^{wt/gt}$ mice (N= 4). The BMDC was activated with DMXAA at 0, 3, and 6 hours. The band is shown in STING protein and phosphorylation of STING at Ser357. (B) Mass spectra of phosphorylation of STING at Ser357 of activated BMDC from *Fcgr2b*$^{-/-}$. *Sting*$^{wt/gt}$ mice after stimulated with DMXAA for 3 hours and followed by immunoprecipitation with Sting. (C) Sting-activated BMDC were co-cultured with PP2 (Lyn inhibitor) and analyzed by flow cytometry. The mean fluorescence intensity (MFI) of IAb expressing DC from *Fcgr2b*$^{-/-}$. *Sting*$^{wt/gt}$ mice is shown (N = 4 mice per group). Data show as mean ± SEM; *p < 0.05. (D-F) Supernatants were collected and analyzed after DMXAA stimulation with or without PP2 inhibitor for 3 hours. Cytokines in the supernatant were detected by cytometric bead array shows the levels of (D) IFN-γ, (E) TNF-α and (F) MCP-1 (N=3-4). Data show as mean ± SEM; *p < 0.05, **p<0.01 and ***p<0.001.

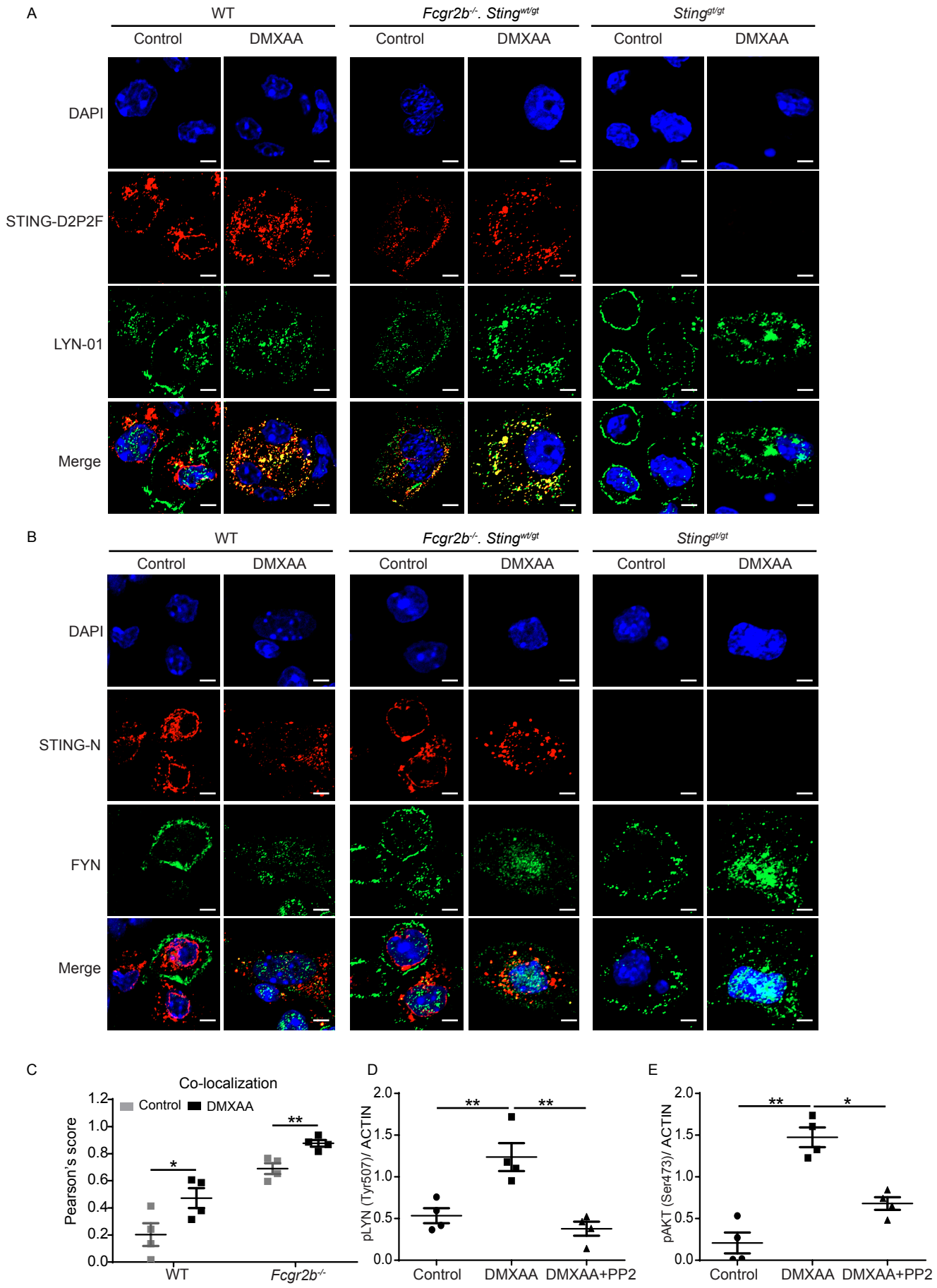

Figure S5. STING activation induces the co-localization with LYN in the differentiation of BMDC, Related to Figure 6. (A-B) The confocal microscope of DMXAA activated BMDC from WT, *Fcgr2b*$^{-/-}$. *Sting*$^{wt/gt}$ and *Sting*$^{gt/gt}$ mice for 6 hours. (A) Staining BMDC with Lyn (01) in green, STING-C (D2P2F) in red, and DAPI in blue is shown. (B) Staining BMDC with Fyn in green, Sting-N in red, and DAPI in blue (scale bar=20 um). The representative of 5 experiments is shown. (C) Co-localization score of STING and LYN were analyzed by ZEISS ZEN Microscope Software (Carl Zeiss, Germany) (N=4 mice per group). (D) Quantification of western blot of (D) pLYN (Tyr507) and (E) pAKT (Ser473) were analyzed by ImageJ software. Data show as mean± SEM; *p < 0.05, **p<0.01, and ***p<0.001.

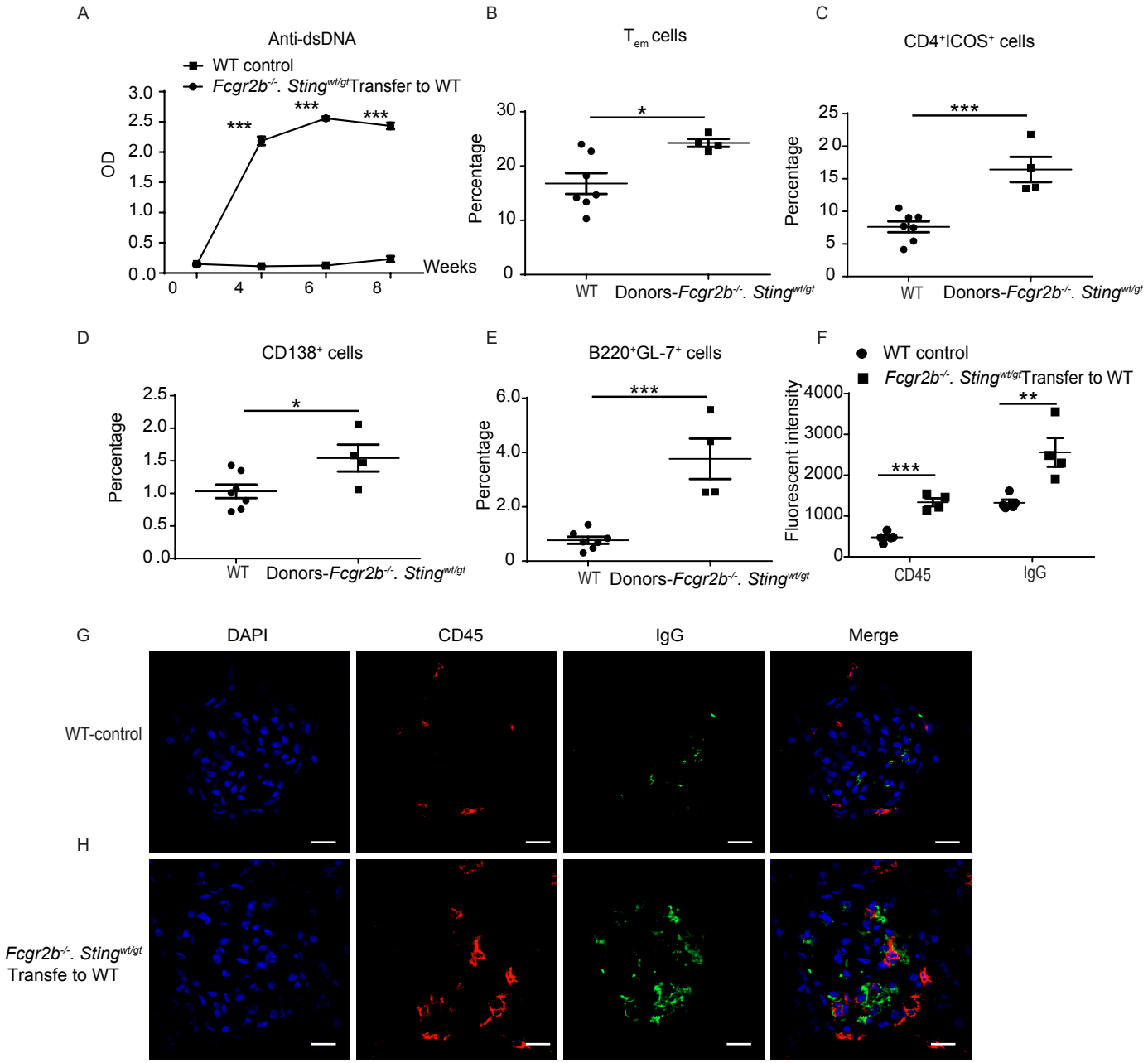

Figure S6. Adoptive transfer of Sting expressing BMDC induces autoimmunity in WT mice, Related to Figure 7.
Transfer of DMXAA activated BMDC from *Fcgr2b*$^{-/-}$. *Sting*$^{wt/gt}$ were transferred into the recipient WT mice. (A) The level of anti-dsDNA from the sera (1:100) measured by ELISA (N=4-5 per group) were tested every 2 weeks after transfer. (B-E) Flow cytometry analysis of recipient splenocytes after BMDC transferred every 2 weeks for 4 times show the percentage of (B) effector T cells (CD4^{+}CD44^{hi}CD62L^{lo}), (C) CD4^{+}ICOS^{+} cells, (D) CD138^{+} cells, and (E) B220^{+}GL7^{+} cells (N=4-7 per group). (F) Quantification of fluorescence intensity of CD45 and IgG were analyzed by ZEISS ZEN Microscope Software (Carl Zeiss, Germany) (N=4-5 mice per group). Data show as mean ± SEM; *p < 0.05, **p<0.01 and ***p<0.001. (G-H) Immunofluorescence staining on the kidneys of IgG in green, CD45 in red, and DAPI in blue from (G) non-transferred WT mice and (H) Fcgr2b$^{-/-}$. Sting$^{wt/gt}$ recipient WT mice are shown. Data are representative of 4-5 mice per group (scale bar=10 μm).

Table S2. Lists of STING interacting proteins, Related to Figure 6

Accession	Gene name	Description
P60710	Actb	Actin, cytoplasmic 1 [OS=Mus musculus]
Q922U2	Krt5	Keratin, type II cytoskeletal 5 [OS=Mus musculus]
P50446	Krt6a	Keratin, type II cytoskeletal 6A [OS=Mus musculus]
Q6IME9	Krt72	Keratin, type II cytoskeletal 72 [OS=Mus musculus]
Q9Z2K1	Krt16	Keratin, type I cytoskeletal 16 [OS=Mus musculus]
P05213	Tuba1b	Tubulin alpha-1B chain [OS=Mus musculus]
P21956	Mfge8	Lactadherin [OS=Mus musculus]
Q8BFR5	Tufm	Elongation factor Tu, mitochondrial [OS=Mus musculus]
Q3UV17	Krt76	Keratin, type II cytoskeletal 2 oral [OS=Mus musculus]
Q3TBT3	Tmem173	Isoform 2 of Stimulator of interferon genes protein [OS=Mus musculus]
P20152	Vim	Vimentin [OS=Mus musculus]
P13020	Gsn	Gelsolin [OS=Mus musculus]
Q3TRJ4	Krt26	Keratin, type I cytoskeletal 26 [OS=Mus musculus]
O35744	Chil3	Chitinase-like protein 3 [OS=Mus musculus]
Q9QWL7	Krt17	Keratin, type I cytoskeletal 17 [OS=Mus musculus]
P01027	C3	Complement C3 [OS=Mus musculus]
P62631	Eef1a2	Elongation factor 1-alpha 2 [OS=Mus musculus]
E9Q557	Dsp	Desmoplakin [OS=Mus musculus]
P62737	Acta2	Actin, aortic smooth muscle [OS=Mus musculus]
Q8C669	Peli1	E3 ubiquitin-protein ligase pellino homolog 1 [OS=Mus musculus]
P01029	C4b	Complement C4-B [OS=Mus musculus]
Q3UHH1	Zswim8	Zinc finger SWIM domain-containing protein 8 [OS=Mus musculus]
P47856	Gfpt1	Glutamine--fructose-6-phosphate aminotransferase [isomerizing] 1 [OS=Mus musculus]
P70248	Myo1f	Unconventional myosin-If [OS=Mus musculus]
Q5SUA5	Myo1g	Unconventional myosin-Ig [OS=Mus musculus]
Q9WTI7	Myo1c	Unconventional myosin-Ic [OS=Mus musculus]
P57780	Actn4	Alpha-actinin-4 [OS=Mus musculus]
Q9CZU3	Mtrex	Superkiller viralicidic activity 2-like 2 [OS=Mus musculus]
Q9CYA6	Zcchc8	Zinc finger CCHC domain-containing protein 8 [OS=Mus musculus]
Q9QXS1	Plec	Plectin [OS=Mus musculus]
Q8VDD5	Myh9	Myosin-9 [OS=Mus musculus]
P62830	Rpl23	60S ribosomal protein L23 [OS=Mus musculus]
P01942	Hba	Hemoglobin subunit alpha [OS=Mus musculus]
Q9WV32	Arpc1b	Actin-related protein 2/3 complex subunit 1B [OS=Mus musculus]
P62874	Gnb1	Guanine nucleotide-binding protein G(I)/G(S)/G(T) subunit beta-1 [OS=Mus musculus]
P62908	Rps3	40S ribosomal protein S3 [OS=Mus musculus]
Q9CPR4	Rpl17	60S ribosomal protein L17 [OS=Mus musculus]
Q9CYL5	Glipr2	Golgi-associated plant pathogenesis-related protein 1 [OS=Mus musculus]
P47757	Capzb	Isoform 3 of F-actin-capping protein subunit beta [OS=Mus musculus]
P25444	Rps2	40S ribosomal protein S2 [OS=Mus musculus]
P60867	Rps20	40S ribosomal protein S20 [OS=Mus musculus]
P07356	Anxa2	Annexin A2 [OS=Mus musculus]

Accession	Gene name	Description
Q6ZWN5	Rps9	40S ribosomal protein S9 [OS=Mus musculus]
P35700	Prdx1	Peroxiredoxin-1 [OS=Mus musculus]
P15331	Prph	Isoform 3u of Peripherin [OS=Mus musculus]
P62702	Rps4x	40S ribosomal protein S4, X isoform [OS=Mus musculus]
Q8CGP2	Hist1h2bp	Isoform 2 of Histone H2B type 1-P [OS=Mus musculus]
Q60765	Atf3	Cyclic AMP-dependent transcription factor ATF-3 [OS=Mus musculus]
Q3V132	Slc25a31	ADP/ATP translocase 4 [OS=Mus musculus]
P58137	Acot8	Acyl-coenzyme A thioesterase 8 [OS=Mus musculus]
P62267	Rps23	40S ribosomal protein S23 [OS=Mus musculus]
P59999	Arpc4	Actin-related protein 2/3 complex subunit 4 [OS=Mus musculus]
P14131	Rps16	40S ribosomal protein S16 [OS=Mus musculus]
P08752	Gnai2	Guanine nucleotide-binding protein G(i) subunit alpha-2 [OS=Mus musculus]
Q64444	Ca4	Carbonic anhydrase 4 [OS=Mus musculus]
Q9DC51	Gnai3	Guanine nucleotide-binding protein G(k) subunit alpha [OS=Mus musculus]
Q9D8B3	Chmp4b	Charged multivesicular body protein 4b [OS=Mus musculus]
Q8VED5	Krt79	Keratin, type II cytoskeletal 79 [OS=Mus musculus]
P11928	Oas1a	2'-5'-oligoadenylate synthase 1A [OS=Mus musculus]
Q9R0N7	Syt7	Isoform 4 of Synaptotagmin-7 [OS=Mus musculus]
P99024	Tubb5	Tubulin beta-5 chain [OS=Mus musculus]
P68372	Tubb4b	Tubulin beta-4B chain [OS=Mus musculus]
P68369	Tuba1a	Tubulin alpha-1A chain [OS=Mus musculus]
P68368	Tuba4a	Tubulin alpha-4A chain [OS=Mus musculus]
Q62191	Trim21	E3 ubiquitin-protein ligase TRIM21 [OS=Mus musculus]
Q9JJZ2	Tuba8	Tubulin alpha-8 chain [OS=Mus musculus]
Q99JY9	Actr3	Actin-related protein 3 [OS=Mus musculus]
P54987	Acod1	Cis-aconitate decarboxylase [OS=Mus musculus]
Q8JZX4	Rbm17	Splicing factor 45 [OS=Mus musculus]
P19973	Lsp1	Lymphocyte-specific protein 1 [OS=Mus musculus]
P25911	Lyn	Tyrosine-protein kinase Lyn [OS=Mus musculus]
P16951	Atf2	Cyclic AMP-dependent transcription factor ATF-2 [OS=Mus musculus]
Q9R112	Sqor	Sulfide:quinone oxidoreductase, mitochondrial [OS=Mus musculus]
P60843	Eif4a1	Eukaryotic initiation factor 4A-I [OS=Mus musculus]
P97793	Alk	ALK tyrosine kinase receptor [OS=Mus musculus]
P61161	Actr2	Actin-related protein 2 [OS=Mus musculus]
P16460	Ass1	Argininosuccinate synthase [OS=Mus musculus]
Q925I1	Atad3	ATPase family AAA domain-containing protein 3 [OS=Mus musculus]
P63017	Hspa8	Heat shock cognate 71 kDa protein [OS=Mus musculus]
Q64213	Sf1	Splicing factor 1 [OS=Mus musculus]
Q6NXH9	Krt73	Keratin, type II cytoskeletal 73 [OS=Mus musculus]
Q02257	Jup	Junction plakoglobin [OS=Mus musculus]
Q91YQ5	Rpn1	Dolichyl-diphosphooligosaccharide--protein glycosyltransferase subunit 1 [OS=Mus musculus]
P38647	Hspa9	Stress-70 protein, mitochondrial [OS=Mus musculus]
Q8BMJ8	Sp8	Transcription factor Sp8 [OS=Mus musculus]
Q62167	Ddx3x	ATP-dependent RNA helicase DDX3X [OS=Mus musculus]

Accession	Gene name	Description
Q9WUA3	Pfkp	ATP-dependent 6-phosphofructokinase, platelet type [OS=Mus musculus]
A2BIM8	Mup18	major urinary protein 18 [OS=Mus musculus]
Q8K1L0	Creb5	Cyclic AMP-responsive element-binding protein 5 [OS=Mus musculus]
Q9WUM4	Coro1c	coronin-1C [OS=Mus musculus]
Q61233	Lcp1	Plastin-2 [OS=Mus musculus]
P20029	Hspa5	78 kDa glucose-regulated protein [OS=Mus musculus]
Q7TPR4	Actn1	Alpha-actinin-1 [OS=Mus musculus]
E9Q634	Myo1e	Unconventional myosin-Ie [OS=Mus musculus]
Q9WU78	Pdcd6ip	Isoform 3 of Programmed cell death 6-interacting protein [OS=Mus
Q6IFX2	Krt42	Keratin, type I cytoskeletal 42 [OS=Mus musculus]
O55143	Atp2a2	Sarcoplasmic/endoplasmic reticulum calcium ATPase 2 [OS=Mus musculus]
P11499	Hsp90ab1	Heat shock protein HSP 90-beta [OS=Mus musculus]
P97449	Anpep	Aminopeptidase N [OS=Mus musculus]
Q9Z331	Krt6b	Keratin, type II cytoskeletal 6B [OS=Mus musculus]
O35691	Pnn	Pinin [OS=Mus musculus]
Q9JKF1	Iqgap1	Ras GTPase-activating-like protein IQGAP1 [OS=Mus musculus]
Q99104	Myo5a	Unconventional myosin-Va [OS=Mus musculus]
Q6R891	Ppp1r9b	Neurabin-2 [OS=Mus musculus]
Q8BTM8	Flna	Filamin-A [OS=Mus musculus]
Q80SU7	Gvin1	Interferon-induced very large GTPase 1 [OS=Mus musculus]
Q0P678	Zc3h18	Zinc finger CCCH domain-containing protein 18 [OS=Mus musculus]
B2RQC6	Cad	CAD protein [OS=Mus musculus]
Q8CH25	Sltm	SAFB-like transcription modulator [OS=Mus musculus]
P62983	Rps27a	Ubiquitin-40S ribosomal protein S27a [OS=Mus musculus]

Transparent Methods

Animals and mouse model

The *Fcgr2b*- deficient mice on the 129/ C57BL/ 6 background (MGI Cat# 2448997, RRID: MGI: 2448997) were obtained from Dr. Bolland (NIH, Maryland, USA). Sting-deficient mice (MGI Cat# 4939598, RRID: MGI: 4939598) were provided by Paludan (Aarhus University, Aarhus, Denmark). Wild type (WT) mice were purchased from the National Laboratory Animal Center, Nakornpathom, Thailand. The *Fcgr2b*- deficient mice were crossed with *Sting*- deficient mice to generate the double-deficient mice and their littermate controls. The double-deficient mice were aged up to 12 months and observed survival compared to their littermates. The animal protocols were approved by the Animal Experimentation Ethics Committee of Chulalongkorn University Medical School.

Measurement of autoantibody

Blood was collected from the mice at the age of 6- 7 months. The levels of anti-dsDNA

from sera (dilution 1:100) were measured by Enzyme-linked immunosorbent assay (ELISA). The anti-nuclear antibodies in serum (dilution 1:800) were detected by indirect immunofluorescence using HEp- 2 cells (EUROIMMUN, Luebeck, Germany). Samples were showed fluorescence intensity and blindly graded as 4= maximal fluorescence (brilliant yellow-green), 3 = less brilliant (yellow- green fluorescence), 2= definite (dull yellow- green), and 1= very dim (subdued fluorescence).

Measurement of cGAMP production

Total splenocytes were isolated from WT, *Sting*-deficient, *Fcgr2b*-deficient, and double deficient mice. Spleens were dispersed through a cell strainer to generate a single-cell suspension and eliminated red blood cells by osmotic shock (ACK buffer: NH_4Cl, $KHCO_3$, and EDTA). The splenocytes were lysed in M-PER™ extraction buffer (Thermo Fisher Scientific, MA USA) (20 x 10^6 cells/100 ul of lysis buffer). cGAMP in cells lysate was measured using 2'3'-cGAMP ELISA Kit (Cayman Chemical, Michigan, USA) according to the manufacturer's instructions. In brief, the ELISA plate contain a blanks (Blk), Total Activity (TA), non-specific binding wells (NSB), maximum binding wells (B0), an eight-point of standard curve and samples (cells lysates). Then, add 50 ul of 2'3'-cGAMP-HRP Tracer to each well except the Total Activity (TA) and the Blank (Blk) wells and add 50 ul of 2'3'-cGAMP Polyclonal Antiserum to each well except the TA, NSB, and the Blk wells. Then cover the plate with plastic film and incubate overnight at 4°C. After incubation, the plates were washed five times with 1x wash buffer, dried, and added 175 µl of TMB substrate solution, then incubated at room temperature for 30 minutes. The stop solution was then added (75 ul), and the absorbance was measured by Varioskan Flash Microplate Reader at 450 nm. (Thermo Fisher Scientific, MA USA).

Cytokines detection

Cytokine panels in serum including IL-1α, IL-1β, IL-6, IL-10, IL-12p70, IL-17A, IL-23, IL-27, MCP-1, IFN-β, IFN-γ, TNF-α, and GM-CSF were measured using LEGENDplex™ Mouse Inflammation Panel kit (Biolegend, San Diego, CA, USA) according to the manufacturer's instructions. The beads were read on a flow cytometer using BDTM LSR-II (BD Biosciences, USA) and analyzed by LEGENDplexTM Data Analysis Software.

Single-cell preparations

Splenic cells were isolated from all experimental groups and littermate WT mice. Spleens were dispersed through a cell strainer to generate a single-cell suspension and eliminated red blood cells by osmotic shock (ACK buffer: NH_4Cl, $KHCO_3$, and EDTA). $CD4^+$ T cells and naïve T cells were isolated from spleen using CD4 isolation Kit and naïve $CD4^+$ T cell Isolation Kit (Miltenyi, Bergisch Gladbach, Germany) as per manufacturer's instructions.

Flow cytometry analysis

The splenocytes (1×10^6 cells) were stained with flow antibody including anti-CD4 (clone: GK1.5; cat.100423), CD8 (clone: 53-6.7; cat. 100708), CD62L (clone: MEL-14; cat. 104417), CD44 (clone: IM7; cat.103035), CD3ε (clone: 145-2C11; cat.100312), ICOS (clone: C398.4A; cat. 313517), CD11c (clone: N418; cat. 117312), B220 (clone: RA3-6B2; cat. 103222), CD11b (clone: M1/70; cat. 101228), I-Ab (clone: AF6-120.1; cat. 116406), PDCA-1 (clone: 129c1; cat.127103), CD80 (clone: 16-10A1; cat. 104733), GL7 (clone: GL7; cat. 144604), CD138 (clone:281-2; cat. 142506) (Biolegend, San Diego, CA, USA). The flow cytometry was performed using BD™ LSR-II (BD Biosciences, USA) and analysis by FlowJo software (USA).

Intracellular staining of T cell was performed as the following method. $CD4^+$ cells (2×10^5 cells) were plated in 200 µl of complete medium supplemented with 25 ng/ml PMA, 1 µg/ml ionomycin (Sigma-Aldrich, Darmstadt, Germany) and 1X GolgiPlug (brefeldin A, Biolegend). After 4 hours of incubation at 37^0C and 5% CO_2, cells were collected and stained with anti-CD3, anti-CD4, anti-CD28, and ICOS before following the cytokines intracellular staining. Briefly, after performed cell surface antigen staining, cells were fixed in 200 µl of fixation buffer (Biolegend) in the dark at 4^0C overnight. Cells were washed three times with 1X permeabilization buffer (Biolegend) and resuspend fixed/permeabilized cells in 50 µl of 1X permeabilization buffer, then added the fluorophore-conjugated antibody for anti- IFN-γ (clone: XMG1.2: cat. 505821) (Biolegend, San

Diego, CA, USA). The flow cytometry was performed using BD™ LSR- II (BD Biosciences, USA) and analysis by FlowJo software (USA).

Gene expression analysis

A total of RNA was extracted from the kidneys and spleen by Trizol reagent (Invitrogen, CA, USA) as per manufacturer's instructions followed by RNA purified using the RNeasy mini kit and treated with DNase I (Qiagen, MD, USA). Then, 1 µg of total RNA was used as a template for cDNA synthesis using iScript RT Supermix (Biorad, California, USA). The expression of interest genes was assessed by quantitative real-time PCR. The gene expression profiles were tested using SsoAdvanced Universal SYBR Green Supermix (Biorad, California, USA). The thermal cycling conditions are as follows: 1 cycle of 95 0C for 5 minutes, followed by 40 cycles of 95 0C for 15 seconds and 60 0C for 1 minute. The relative amounts of target mRNA will be normalized to β-actin mRNA as a housekeeping gene and determined by the $2^{(-ddCt)}$. Microarray analysis was performed by RNA labeling and hybridization using the Agilent One-Color Microarray- Based Gene Expression Analysis protocol (Agilent Technology, V 6. 5, 2010). Microarray results were extracted using Agilent Feature Extraction software v11. 0 (Agilent Technologies, Palo Alto, USA).

Immunofluorescence and Histopathology

Frozen renal sections were fixed in acetone and blocked with 1% BSA in PBS. After that, the sections were stained with FITC-conjugated goat anti- mouse IgG antibodies and PE-conjugated goat anti-mouse C45RB antibodies (Abcam, Cambridge, MA, USA). Then, samples were stained with DAPI (4',6- Diamidino- 2- Phenylindole, Dihydrochloride) (Thermo Fisher Scientific, MA USA) for 5 minutes in the dark at room temperature. Slides were washed three times and mounted with ProLongTM diamond antifade mountant (Invitrogen, CA, USA). The fluorescent signaling was visualized by ZEISS LSM 800 with Airyscan (Carl Zeiss, Germany).

For determine the $CD45^{+}$ cell deposition and C3 deposition in the kidney, the sections were stained with anti-C3c antibody (FITC; cat. Ab4212) (Abcam, Cambridge, MA, USA), Alexa Fluor® 647 anti-mouse CD3 (clone: 17A2; cat. 100209) Antibody and Alexa Fluor® 647 anti-mouse CD11c (clone: N418; cat. 117312) (Biolegend, San Diego, CA, USA). Then, samples were stained with DAPI, as described above. The quantification of fluorescence intensity was analyzed by ZEISS ZEN Microscope Software (Carl Zeiss, Germany). The deparaffinized kidney sections were fixed with formalin subsequently stained with H&E. The pathology grading from kidney sections was blinded analysis by the nephrologist.

Cell preparation for in vitro assay

Differentiation of bone marrow-derived dendritic cell (BMDC) was performed as follows. Bone marrow cells were obtained from the femur. Cells were cultured in RPMI 1640 supplemented with 10 % FBS, 1 mM Na pyruvate, 10 mM HEPES buffer, 1% L-glutamine, 1% nonessential amino acid, 100 units/ml pen/ strep (Gibco-Thermo Fisher Scientific, MA USA) and 50 µM 2-mercaptoethanol (Sigma-Aldrich, Darmstadt, Germany). Cells were stimulated with IL-4 (20 ng/ml) and GM-CSF (20 ng/ml) (Miltenyi, Bergisch Gladbach, Germany) and maintained at 370C in a CO2 incubator for five days. The immature dendritic cells were activated by adding 10 µg/ml of DMXAA (5,6-Dimethylxanthenone-4-acetic acid or STING ligand) (Invivogen, San Diego, USA) for 24 hours. The mature BMDC and collected supernatant were stained with the antibodies and analyzed by flow cytometer. For cGAMP activation,BMDC from WT, *Sting*$^{gt/gt}$, *Fcgr2b*$^{-/-}$ and *Fcgr2b*$^{-/-}$. *Sting*$^{gt/gt}$ were cultured, as described above. The immature dendritic cells were transfected with 4 µg/ml of 2'3'-cGAMP (cyclic GMP-AMP; c-GpAp) (Invivogen, San Diego, USA) by lipofectamine P3000 Reagent (Thermo Fisher Scientific, MA USA) as per manufacturer's instructions for 24 hours. The mature BMDC were stained with the antibodies and analyzed by flow cytometer.

CFSE (Carboxyfluorescein succinimidyl ester) labeling was performed as described below. T cells (1x 10^6) in pre-warmed (37^0C) in PBS were incubated with 0. 5 µM CFSE (Biolegend, San Diego, CA, USA) at 37^0C in a CO_2 incubator for 10 minutes. Cells were quench labeling reaction with ten volumes of complete ice-cold medium and centrifuged for 5 minutes at 1,500 rpm, 4^0C. Labeled cells were washed by resuspending in a complete medium. CFSE labeled cells are now ready for in vitro culture.

In vitro co-cultures of BMDCs and T cells

BMDCs were cultured with T cells for 6 hours. Briefly, immature BMDCs were cultured and activated with DMXAA (STING ligand) for 24 hours at 37^0C and washed twice before co-culture. Activated BMDCs (4 x 10^4) were plated in 200 µl of complete medium with CD4+ T cells (2 x 10^5) from lymph nodes (1:5; 4 x10^4 DC: 2 x 10^5 T cells) for 6 hr at 37^0C and 5% CO_2 followed by intracellular staining for anti-IFN-γ as described above. For proliferation assays, naïve T cells were labeled with CFSE as described above, according to the manufacturer's instruction (Biolegend, San Diego, CA, USA), before co-cultured with activated BMDCs. In brief, activated BMDCs (4 x 10^4) were plated in 200 µl of complete medium with naïve T cells (2 x 10^5) from spleen (1:5, 4 x10^4 DC: 2 x 10^5 T cells) for 72 hours at 37^0C and 5% CO_2. After co-culture, T cells were stained with intracellular cytokine for anti-IFN-γ and detect their proliferation by dilution of CFSE fluorescence by flow cytometer.

Colocalization of STING and LYN in BMDC cells

Immature BMDCs from WT and *Fcgr2b*$^{-/-}$ were cultured, then stimulated with DMXAA for 6 hr. Cells were fixed with 4% formalin (Sigma-Aldrich, Darmstadt, Germany) at room temperature for 15 minutes. Incubate the fixed cells for 10 min with 0.2% Triton X-100 and block unspecific binding of the antibodies with 0.1% BSA for 1 hour BMDCs were probed with anti-LYN antibody (cat. 2732, Cell Signaling, MA, USA) and anti-FYN antibody [FYN-01] (cat. 1881, Abcam, Cambridge,

MA, USA) for overnight at 4 ^{0}C. After incubation, secondary antibody Alexa Fluor 488 rabbit IgG (Thermo Fisher Scientific, MA, USA) was added for 1 hour at room temperature. For STING detection, STING antibody was incubated with Zenon™ Alexa fluor™ 555 rabbit IgG labeling kit (Thermo Fisher Scientific, MA, USA) and then stained the BMDCs. The cells were subsequently probed with 1 µM DAPI (Thermo Fisher Scientific, MA USA) for 5 minutes, and the fluorescent signaling was visualized by ZEISS LSM 800 with Airyscan (Carl Zeiss, Germany). To confirm the specificity of the antibody, BMDCs were probed with LYN antibody (clone Lyn-01; cat MAB0949) (1:200) (Abnova,Taipei, Taiwan) and STING-C antibody (clone D2P2F, cat: 13647) (Cell Signaling, MA, USA) as described above. The colocalization score was analyzed by ZEISS ZEN Microscope Software (Carl Zeiss, Germany).

Sample preparation for MS analysis

Quantitative proteomic analysis of mature BMDC was studied using a dimethyl labeling method (Makjaroen et al., 2018). Briefly, BMDC were cultured and then stimulated with 10 µg/ml of DMXAA (STING ligand) for 24 hours. Three hundred microgram proteins per group from BMDC were digested overnight at 37 ^{0}C with trypsin [1:50 (w/w)]. Next, stimulated BMDC's peptides from WT mice, *Fcgr2b*$^{-/-}$ mice, and *Fcgr2b*$^{-/-}$.*Sting*$^{gt/gt}$ mice were labeled with light reagents [formaldehyde (Sigma) and sodium cyanoborohydride (Sigma)], medium reagents [formaldehyde-d2 (CIL) and sodium cyanoborohydride], and heavy reagents [deuterated and 13C-labeled formaldehyde (Sigma) and cyanoborodeuteride (CIL)], respectively, for an hour at room temperature. The peptides were fractionated and subjected to LC-MS/MS (Thermo). Unpaired t-tests determined significantly differentially regulated proteins (with p-value < 0.05 considered significant).

For proteomics analysis, the WT mice channels were used as denominators to generate abundance ratios of *Fcgr2b*$^{-/-}$ mice/ WT mice and *Fcgr2b*$^{-/-}$.*Sting*$^{gt/gt}$ mice/ WT mice**.** Log2 of the

normalized ratio was used to calculate the mean and standard deviation of fold change across all four biological replicates. When these ratios were found in less than three experiments, the relevant proteins were excluded. To analysis the up- and down-regulated proteins, the ratios of *Fcgr2b*$^{-/-}$/*Fcgr2b*$^{-/-}$.*Sting*$^{gt/gt}$ mice were performed. Unpaired t-tests determined significantly differentially regulated proteins with p-value < 0.05 considered significant. The online resource Database for Annotation, Visualization, and Integrated Discovery (DAVID, v 6. 8, https://david.ncifcrf.gov/), and interferome (http://www.interferome.org/) was employed to classify the vital proteins into functional categories and interferon regulated proteins using all proteins identified by MS as background (for DAVID).

Isolation of T cells from the lymph node and spleen

Lymph nodes and spleens were removed from sacrificed mice and littermate wild-type mice. Lymph nodes and spleens were dispersed through a cell strainer to generate a single-cell suspension as described above. T cells were isolated and purified using $CD4^+$ T Cells Isolation Kit (Miltenyi, Bergisch Gladbach, Germany) as per manufacturer's instructions. Briefly, splenocytes and total cells from lymph nodes were prepared (2 x 107) and incubated with 20 µl of Biotin-Antibody Cocktail for 5 minutes at 4 ^{0}C. Then, the mixed cells were incubated with 40 µl of Anti- Biotin MicroBeads for 10 minutes at 4 ^{0}C, and proceed to subsequent magnetic cell separation (Miltenyi, Bergisch Gladbach, Germany). The viability and purity of purified CD4+ T cells were stained with anti-CD3, anti-CD4 (Biolegend, San Diego, CA, USA) and Fixable Viability Dye eFluor® 780 (Thermo Fisher Scientific, MA USA), then examined by flow cytometer.

Immunoprecipitation of STING-interacting proteins

BMDCs from WT, *Fcgr2b*$^{-/-}$ and *Sting*$^{gt/gt}$ were cultured, then stimulated with DMXAA for 3 hr. Cells were collected and lysed with 1 % IGEPAL CA-630, 0.5% TritonX-100, 150 mM NaCl, 50 mM Tris pH 7. 4, 5% glycerol, 100 mM beta-Glycerophosphate, 2 mM Na_3VO_4 and 1X proteases

inhibitor cocktail (Roche) . First, the antibody was mixed with the magnetic beads by adding 10 µg of STING antibody (CUSB in-house antibody, clone: GTN-01; targeted N-terminal) with 400 µg of SureBeads™ Protein A magnetic beads (Biorad, California, USA) and incubated for 1 hour at room temperature. Then, Protein lysates were added and incubated with antibody-conjugated beads for overnight at 4^0C. After incubation, the beads were washed three times with wash buffer (150 mM NaCl and 50 mM Tris- HCl pH 7. 4). Samples were eluted by adding 5X laemmli buffer and boiled 95^0C for 10 minutes. For reverse IP, the antibody was mixed with the magnetic beads by adding 10 µg of LYN antibody (clone Lyn-01; cat MAB0949) (Abnova, Taipei, Taiwan) with 400 µg of SureBeads™ Protein G magnetic beads (Biorad, California, USA) followed by incubated with activated BMDC as described above. The eluted protein samples were separated by 10 % SDS- PAGE gel. The STING-interacting proteins from co- IP were analyzed by in-gel digestion, followed by LC-MS/MS analysis.

Western Blot Analysis

Splenocytes were lysed in 2 % SDS lysis buffer. Lysates were homogenized and centrifuged at 12,000×g for 15 min at 4 ^{0}C. The supernatants were collected, and total protein was measured by BCA protein assay (Thermo Scientific, Illinois, USA). Cell lysates containing equal amounts of protein (20 µg) were boiled in SDS sample buffer at 37 ^{0}C for 15 min before separation on a 10 % SDS-polyacrylamide gel. Proteins were transferred to nitrocellulose membranes and Western blot analysis.

BMDC from WT, *Fcgr2b*$^{-/-}$, and *Sting*$^{gt/gt}$ was cultured and stimulated with DMXAA for 3 hours, as described above. Protein lysates were prepared and run on 10 % SDS-polyacrylamide gel, then proteins were transferred to nitrocellulose membranes and probed with STING antibody (clone: GTN-01; 1:2000) (CUSB-in house, BKK, TH), STING-C antibody (clone D2P2F, cat: 13647) (Cell Signaling, MA, USA), LYN antibody (clone: LYN-01;1:1000) (Biolegend, San Diego, CA, USA) and LYN antibody (cat: 2732) (Cell Signaling, MA, USA). After incubation at 4 ^{0}C for overnight,

the membrane was washed and probed with IRDye® 680RD Donkey anti-Rabbit IgG (H + L) and IRDye® 800CW Donkey anti-Mouse IgG (H + L) secondary antibody (1:10000) (LI-COR, Lincoln, Nebraska, USA) for 1 hour at room temperature. The membrane was determined the signals by ODYSSEY CLx (LI-COR, Lincoln, Nebraska, USA).

Inhibition of LYN in Sting-activated BMDC

BMDC was prepared as described above in the presence of GM-CSF and IL-4 (Miltenyi, Bergisch Gladbach, Germany) in a 100 mm petri dish (at least 5 million cells/dish). On the day of DMXAA stimulation, free and non-adherent cells were flushed off and spun down, counted, and seeded out into 24-well plates (approx. 1 mill cells/well). Cells were then incubated with the LYN inhibitors PP2 (Sigma-Aldrich, Darmstadt, Germany) for one hour before the addition of DMXAA and LPS for 24 hrs, and subsequently stained and fixed for flow cytometry analysis.

For protein expression, total proteins from BMDC were analyzed by Western blotting. Samples were diluted in XT sample buffer and XT reducing agent and ran on an SDS–PAGE (Criterion™ TGX™). Trans-Blot Turbo™ Transfer System® was used for the transfer of proteins to PVDF membranes (all reagents Bio-Rad). The membrane was blocked in 5% Difco™ skim milk (BD). The antibodies used for Western blotting were all from Cell Signaling (Cell Signaling, MA, USA), Phospho-LYN (Tyr507) Rabbit Antibody, CST-2796S, LYN (C13F9) Rabbit mAb, CST-9271S, Phospho-AKT (Ser473) Antibody, and CST-AKT antibody. Quantification of the western blot was analyzed by ImageJ software. For gene expression, a total RNA from BMDC after DMXAA stimulation with or without PP2 inhibitor for 3 hours was isolated by Trizol reagent (Invitrogen, CA, USA) as described above. The interferon signature genes were tested by real-time PCR.

Adoptive transfer

BMDC from WT, *Fcgr2b*$^{-/-}$, and *Fcgr2b*$^{-/-}$.*Sting*$^{gt/gt}$ mice were cultured as described above. The recipient WT or *Fcgr2b*$^{-/-}$.*Sting*$^{gt/gt}$ mice (at the age of 4 months) received approximately 10^6 cells of BMDC via tail vein injection every two weeks per injection for four times. The control, *Fcgr2b*$^{-/-}$.*Sting*$^{gt/gt}$ mice received only sterile PBS (vehicle). Sera were collected, and ELISA measured the levels of anti-dsDNA. Mice were euthanized two weeks after the final transfer (at the age of 6 months).

Statistical analysis

All statistical analyses employed the two-tailed Mann-Whitney test. Statistical analyses were performed using GraphPad Prism 4.0 (GraphPad Software, San Diego, CA).

Supplemental information

Gene expression profiles of the kidneys have been deposited in the Gene expression Omnibus (GEO) website with ID GSE142594 and available at

https://www.ncbi.nlm.nih.gov/geo/query/acc.cgi?acc=GSE142594

The mass spectrometry proteomics data, including annotated spectra for all modified peptides and proteins identified, have been deposited to the ProteomeXchange Consortium via the PRoteomics IDEntifications (PRIDE) partner repository with the data set identifier PXD019239.

Supplemental References

Makjaroen, J., Somparn, P., Hodge, K., Poomipak, W., Hirankarn, N., and Pisitkun, T. (2018). Comprehensive Proteomics Identification of IFN-lambda3-regulated Antiviral Proteins in HBV-transfected Cells. Mol Cell Proteomics *17*, 2197-2215.